

Metamorphic Evolution and Tectonic Implications of the Granulitized Eclogites from the Luliangshan Terrane in the North Qaidam Ultrahigh Pressure Metamorphic Belt, NW China: New Constraints from Phase Equilibrium Modeling

Guisheng Zhou^①, Jianxin Zhang^{②*}, Yunshuai Li², Zenglong Lu¹, Xiaohong Mao¹, Xia Teng¹

1. Key Laboratory of Deep-Earth Dynamics of the Ministry of Land and Resources, Institute of Geology, Chinese Academy of Geological Sciences, Beijing 100037, China

2. Institute of Surface-Earth System Science, Tianjin University, Tianjin 300072, China

① Guisheng Zhou: <https://orcid.org/0000-0002-4672-1036>; ② Jianxin Zhang: <https://orcid.org/0000-0002-5733-8091>

ABSTRACT: The granulitized eclogites from the Luliangshan terrane of the North Qaidam UHP metamorphic belt occur as lenses within pelitic gneisses and orthogneisses. Combined petrologic data and phase equilibrium modeling indicate a multi-stage metamorphic history of the granulitized eclogites: (1) an earlier eclogite facies metamorphism ($P>18.5$ kbar, $T>830$ °C) is deduced from omphacite relics in the matrix and rare omphacite inclusions within garnet. The possible assemblage is garnet+omphacite+rutile+quartz; (2) the early stage of high pressure granulite facies assemblages (garnet+clinopyroxene+plagioclase+rutile+quartz+liquid) developed in the early decompression process has a P - T regime of 17.5 kbar and 852–858 °C, constrained by plagioclase and clinopyroxene inclusions in garnet. The late stage of high pressure granulite assemblages (garnet+clinopyroxene+amphibole+plagioclase+rutile+quartz+liquid) records an isothermal decompression process with the pressure successively declining from 17.5 to 14.7 kbar and to 11.3 kbar at 858 °C; (3) the later medium pressure granulite facies assemblage (garnet+orthopyroxene+clinopyroxene+amphibole+plagioclase+ilmenite+liquid+quartz) indicates a drop in pressure and rise in temperature at P - T conditions of 7.6–7.7 kbar and 878–883 °C; (4) retrogressive amphibolite facies stage, which is represented by amphibole+plagioclase kelyphitic rims around garnet, formed under conditions of <5 kbar and <650 °C. The preservation of medium pressure granulite facies assemblage and the garnet composition feature constrain a following isobaric cooling path during late exhumation. This process suggests a clockwise P - T path and indicates that the granulitized eclogites record a high grade “Barrovian” metamorphic overprint at the middle-lower crust during exhumation. The present data show that the Luliangshan terrane is a “hot” HP-UHP terrane.

KEY WORDS: phase equilibrium modeling, granulitized eclogite, North Qaidam, Luliangshan terrane.

0 INTRODUCTION

The North Qaidam (NQD) ultrahigh pressure (UHP) metamorphic belt is located at the north margin of the Tibet Plateau (Fig. 1). It has been a focus of research as a typical Alpine-type subduction zone for the outcrop of eclogites, peridotites as lens of continental felsic gneisses and the recognition of UHP minerals such as coesite and diamond (Zhang et al., 2017, 2010, 2005; Song et al., 2006, 2003; Yang J S et al., 2002, 2001, 1998; Yang J J et al., 1994). Eclogites from the Luliangshan terrane, the West NQD were initially recognized as high pressure mafic granulites without the recognition of omphacite in the matrix although

omphacite inclusions were observed in garnet (Zhang et al., 2008, 2007). Recently, the omphacite has also been recognized in the matrix of the granulitized eclogite blocks from the Luliangshan terrane (Chen et al., 2018). The strongly retrogressed eclogites from the Luliangshan terrane were commonly regarded as the typical HP-UHP rocks which were overprinted by high-temperature (HT) granulite-facies conditions during decompression (Chen et al., 2018; Cao et al., 2017; Zhang et al., 2008). However, a detailed P - T evolution history has not been obtained. The previous P - T estimate of the granulitized eclogites from the Luliangshan terrane gave a spread temperature gap (730–930 °C) for granulite facies overprint based on conventional thermobarometry. Symplectitic, coronitic and kelyphytic reaction textures are very common in these rocks and witness lack of textural equilibrium, and compositional equilibrium is not attained or only attained at microdominal scale. Phase equilibrium modeling can give a detailed interpretation of the reaction textures and allows a considerable refinement of the metamorphic evolution by solving

*Corresponding author: zjx66@yeah.net

© China University of Geosciences (Wuhan) and Springer-Verlag GmbH Germany, Part of Springer Nature 2019

Manuscript received November 12, 2018.

Manuscript accepted January 5, 2019.

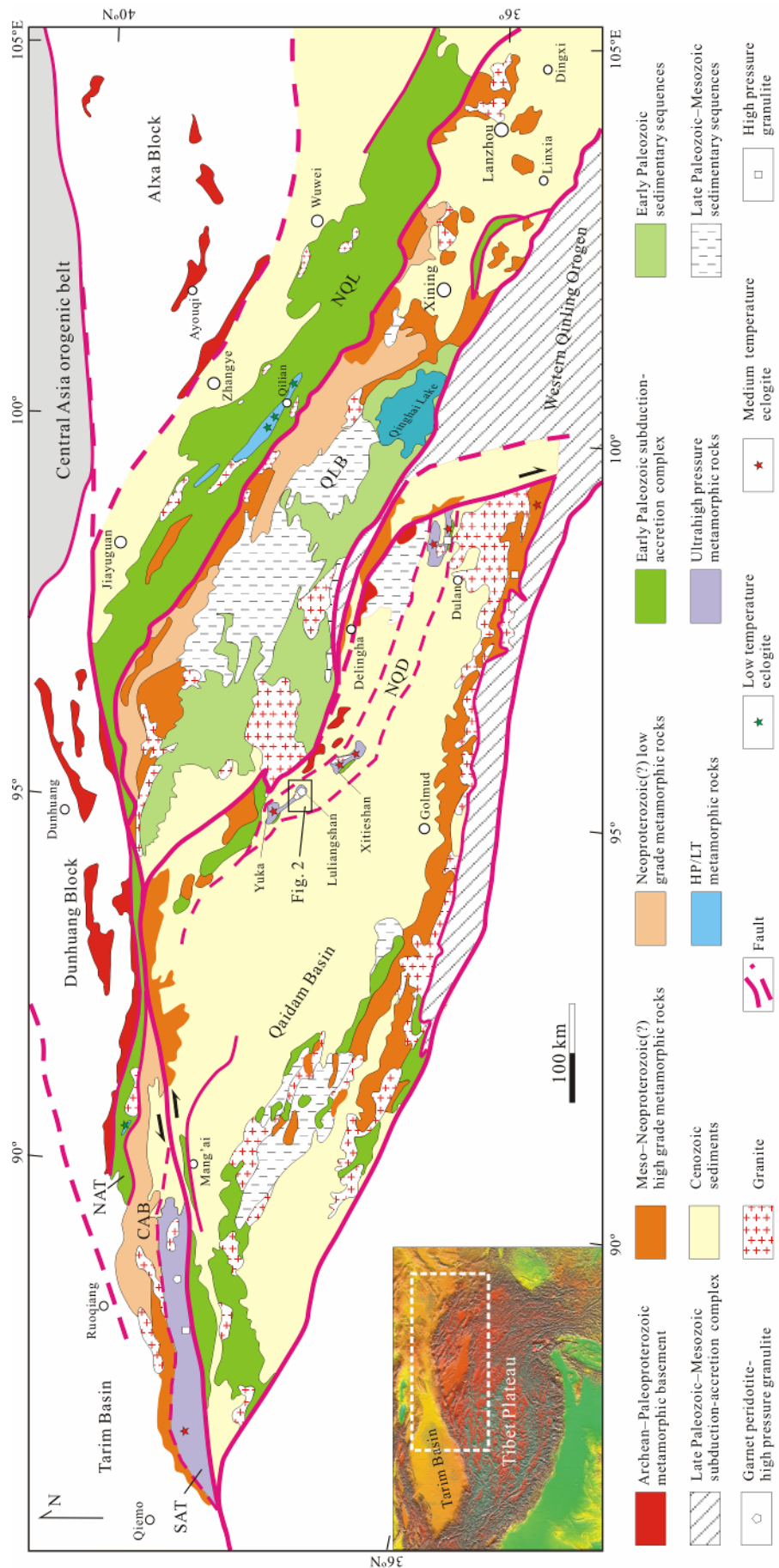


Figure 1. Geological sketch map of the North Qaidam orogenic belt and the adjacent areas in the northern Tibet (modified after Zhang et al., 2017). NQD. North Qaidam subduction-collision complex; SAT. South Altun subduction-collision complex; CAB. Central Altun Block; NQL. North Qilian subduction-accretion complex; QLB. Qilian Block;

the problem of domainal textural and compositional equilibrium (e.g., Groppe et al., 2015; Cruciani et al., 2012). On the other hand, many studies did not consider the presence of liquid (melt) for the lack of appropriate melt model when making the *P-T* estimate of the granulitized mafic rocks by phase equilibrium (e.g., Liao et al., 2016). It is not rigorous to neglect the melt liquid for high grade granulites rocks and the setting of saturated pure water may underestimate the granulite facies temperature. In this paper, we investigated the granulitized eclogites from the Luliangshan terrane based on detailed petrological data and phase equilibrium calculations using the latest melt modal for mafic rocks (Green et al., 2016). We aimed to explore the metamorphic evolution of the granulitized eclogite and illuminate its exhumation process. The results provide precise *P-T* conditions to understand the nature of the tectonic process of the Luliangshan terrane as a part of the NQD UHP metamorphic belt in the Early Paleozoic.

Mineral abbreviations in this paper are mainly after Holland and Powell (1998) and listed as follows: cpx, clinopyroxene; ep, epidote; g, garnet; hb, calcium and sodium-caesium amphibole; ilm, ilmenite; liq, melt liquid; mu, muscovite; opx, orthopyroxene; omp, omphacite; pl, plagioclase; q, quartz; ru, rutile; ilm, ilmenite.

1 REGIONAL GEOLOGY AND FIELD OCCURRENCE

The NQD UHP metamorphic belt is characterized by NWW-SEE linear distribution between the Qaidam Block and the Oulongbuluke (Quanji) microcontinental block, and is cut by the Altyn Tagh sinistral strike-slip fault in the west (Fig. 1). It is mainly composed of continental paragneiss and orthogneiss with minor (retrograde) eclogites, amphibolites and peridotites occurring as blocks or boudins. The UHP rocks are in depositional contact (locally faulted) with the overlying Lower Paleozoic volcanic and sedimentary rocks of the Tanjianshan Group and are intruded by granite plutons. Eclogite blocks disperse over 350 km near the localities of Yuka, Xiteshan and Dulan and record peak metamorphic ages between 420 and 460 Ma (Zhang J X et al.,

2017, 2010, 2005; Yang et al., 2015; Song et al., 2014, 2012, 2010; Yu et al., 2013; Zhang C et al., 2012). Garnet peridotite outcrops in the Luliangshan area and appears to have been exhumed from mantle depths >200 km (Song et al., 2005, 2004). Based on rock associations, petrologic criteria, and field relationships, four UHP metamorphic units can be distinguished along the North Qaidam Mountains (NQD) from east to west (Fig. 1): (1) the Dulan eclogite-gneiss unit (DLU), which consists of granitic gneiss, paragneiss, eclogite, HP granulite and ultramafic lenses enclosed within gneiss; (2) the Xiteshan eclogite-gneiss unit (XTU), dominated by kyanite (sillimanite)-bearing paragneiss and felsic gneiss with rare marble, amphibolite and intruded by granite plutons dated at 428 Ma; (3) the Luliangshan garnet peridotite-granulitized eclogite-gneiss unit (LLU), defined by kyanite (sillimanite)-bearing paragneiss and granitic gneiss with ultramafic rocks (garnet peridotite and garnet pyroxenite) and granulitized eclogites as lenses and intruded by Silurian granite plutons; (4) the Yuka- Luofengpo eclogite-gneiss unit (YKU), which comprises eclogite, metapelite, granitic gneiss and rare marble.

The Luliangshan garnet peridotite-granulitized eclogite-gneiss unit is located ~20 km south of Da Qaidam Town (Fig. 2). It consists of kyanite (or sillimanite)-bearing and garnet-bearing gneisses, orthogneiss, granulitized eclogites lenses (Figs. 3a, 3b), and a garnet peridotite block. Carbonatites were recently recognized and were regarded as evidences for recycling of sedimentary carbonate and mantle metasomatism (Li et al., 2018). This unit is intruded by granite plutons on the western side, and is covered by Quaternary deposits on other sides. Peak metamorphic conditions of 45–50 kbar and 900–1 000 °C have been calculated for the garnet peridotite (Song et al., 2005, 2004). Based on detailed field mapping, the distribution of granulitized eclogites, carbonatites, marbles, ultramafic rocks lens and the relationship between paragneiss and orthogneiss were reconstructed (Fig. 2). The locations of the granulitized eclogite samples including AQ17-14-4, Q07-14-4 and Q05-18e are labeled in Fig. 2.

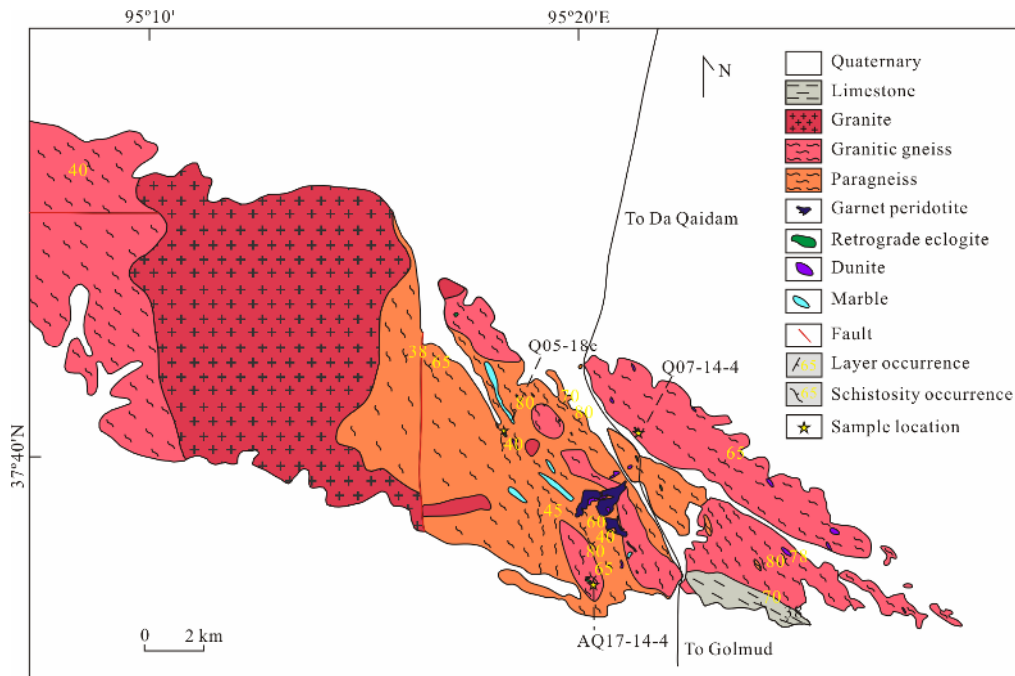


Figure 2. Geological sketch map of the Luliangshan terrane showing the geological setting and sampling locations (modified after Zhang et al., 2007).

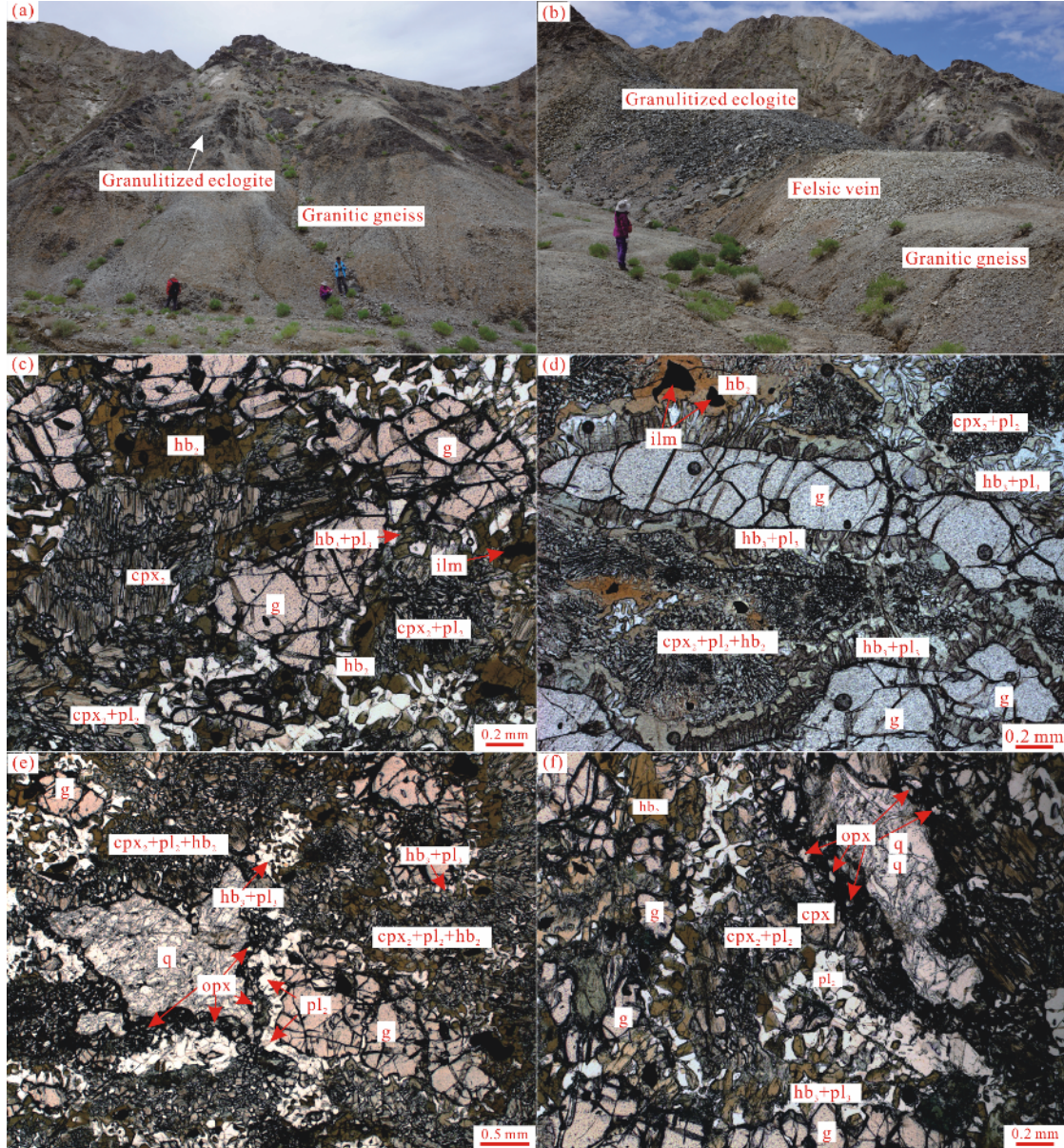


Figure 3. Photographs showing the occurrences and typical textural relationships for the granulitized eclogites. (a) Lenticular granulitized eclogite enclosed in the granitic gneiss; (b) layered granulitized eclogite enclosed in the granitic gneiss; (c) and (d) overview of the granulitized eclogite, $\text{cpx}_2+\text{pl}_2+\text{hb}_2$ symplectites in the matrix and kelyphitic pl_3+hb_3 around garnet porphyroblast; (e) and (f) opx+ pl_2 coronas between garnet and quartz.

2 PETROGRAPHY AND MICROTETURES

The studied granulitized eclogites consist of garnet, clinopyroxene, orthopyroxene, amphibole, plagioclase, minor omphacite and quartz with accessory rutile, ilmenite, and apatite (Figs. 3c–3f, and 4). In our samples, most garnet grains are anhedral and contain some mineral inclusions of omphacite and rutile. Omphacite grains in the matrix are only found in sample AQ17-14-4 (Fig. 4a). Omphacite inclusions are partially replaced by clinopyroxene+plagioclase+amphibole ($\text{cpx}_1+\text{pl}_1+\text{hb}_1$), interpreted as the result of the presence of fluid through fracture of garnet during the decompression stage. Amphiboles are observed in three different textural positions: (1) as inclusions within garnet; (2) as large crystals in the matrix; and (3) as kelyphytic rims around garnet porphyroblasts. Plagioclase observed in the granulitized eclogites can be divided into four textural types: (1) anhedral inclusions intergrown with clinopyroxene in the garnet; (2)

$\text{cpx}+\text{pl}\pm\text{hb}$ symplectite; (3) pl coronas intergrown with opx coronas around garnet porphyroblasts; (4) plagioclase in the kelyphite around garnet porphyroblasts. The prograde metamorphic assemblages have not been observed. On the basis of the microstructures, four metamorphic stages can be recognized: (1) eclogite facies stage; (2) high pressure granulite facies stage; (3) medium pressure granulite facies stage; (4) late amphibolite facies retrograde stage.

2.1 Eclogite Facies Stage (M_1)

The eclogite-facies mineral assemblage includes relict omphacite with high jadeite content, rutile, and quartz that occur as inclusions within garnets. Rare omphacite grains are preserved in the cores of clinopyroxenes in the matrix. These observations suggest an eclogite facies assemblage of $\text{g}+\text{omp}+\text{ru}+\text{q}$.

2.2 High Pressure Granulite Facies Stage (M₂)

The early stage of HP granulite facies was mainly constrained by mineral inclusions (cpx_1+pl_1) in garnets which have fractures

linked to the matrix (Figs. 4c, 4d, 5). The late stage of HP granulite facies assemblages were represented by $\text{cpx}_2+\text{pl}_2+\text{hb}_2$ symplectites in the matrix (Figs. 3c, 3d, 3e, 4a, 4b, 4e, 4f, 4g).

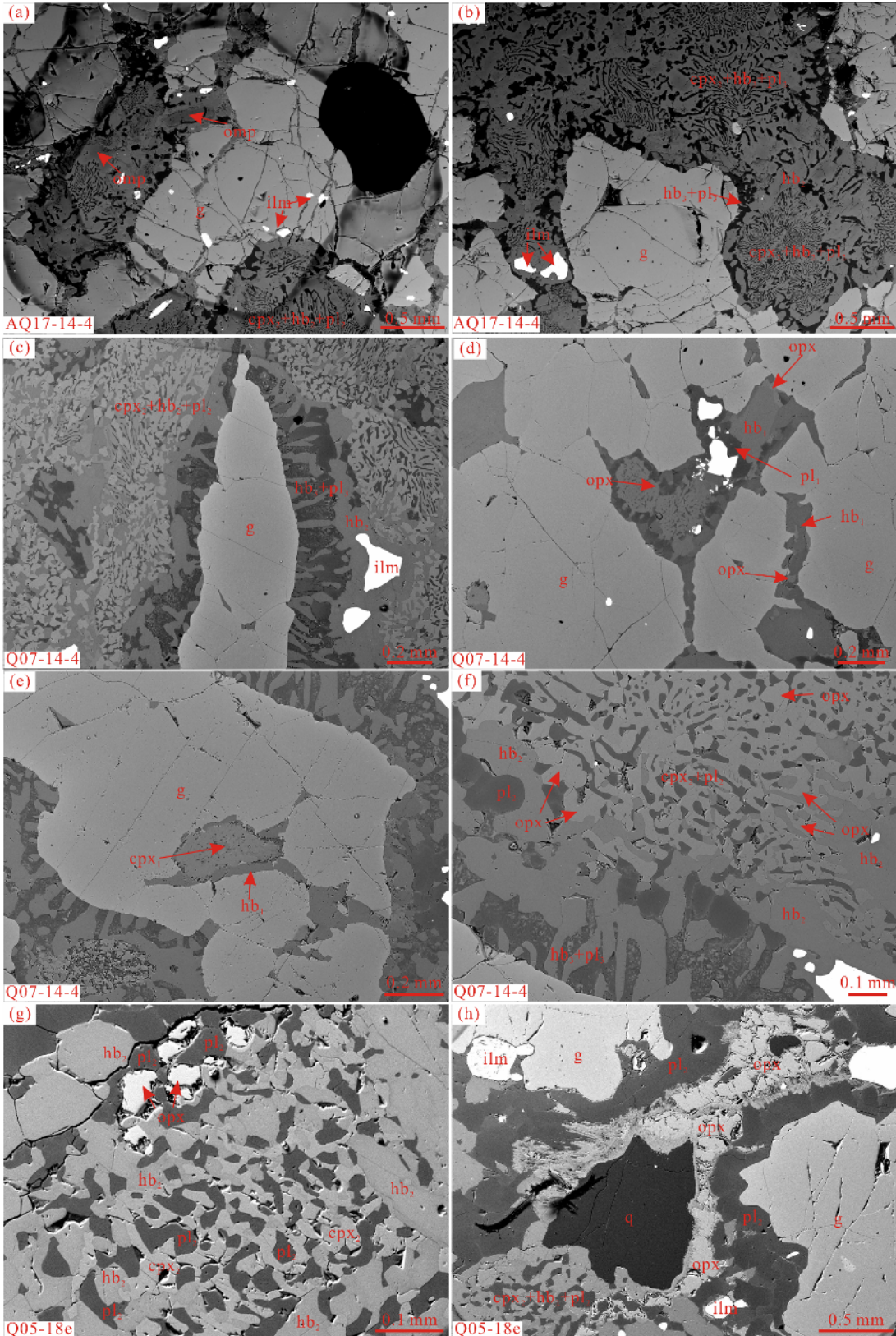


Figure 4. Backscattered electron images showing typical microtextures in the granulitized eclogites. (a) The relict omphacite grains in the matrix; (b) and (c) $\text{cpx}_2+\text{pl}_2+\text{hb}_2$ symplectites in the matrix and pl_3+hb_3 kelyphitic rims; (d) and (e) orthopyroxene, clinopyroxene, plagioclase, amphibole inclusions in garnet; (f) and (g) $\text{cpx}_2+\text{pl}_2+\text{hb}_2+\text{opx}$ symplectites in the matrix; (h) $\text{opx}+\text{pl}_2$ coronas between the garnet and quartz.

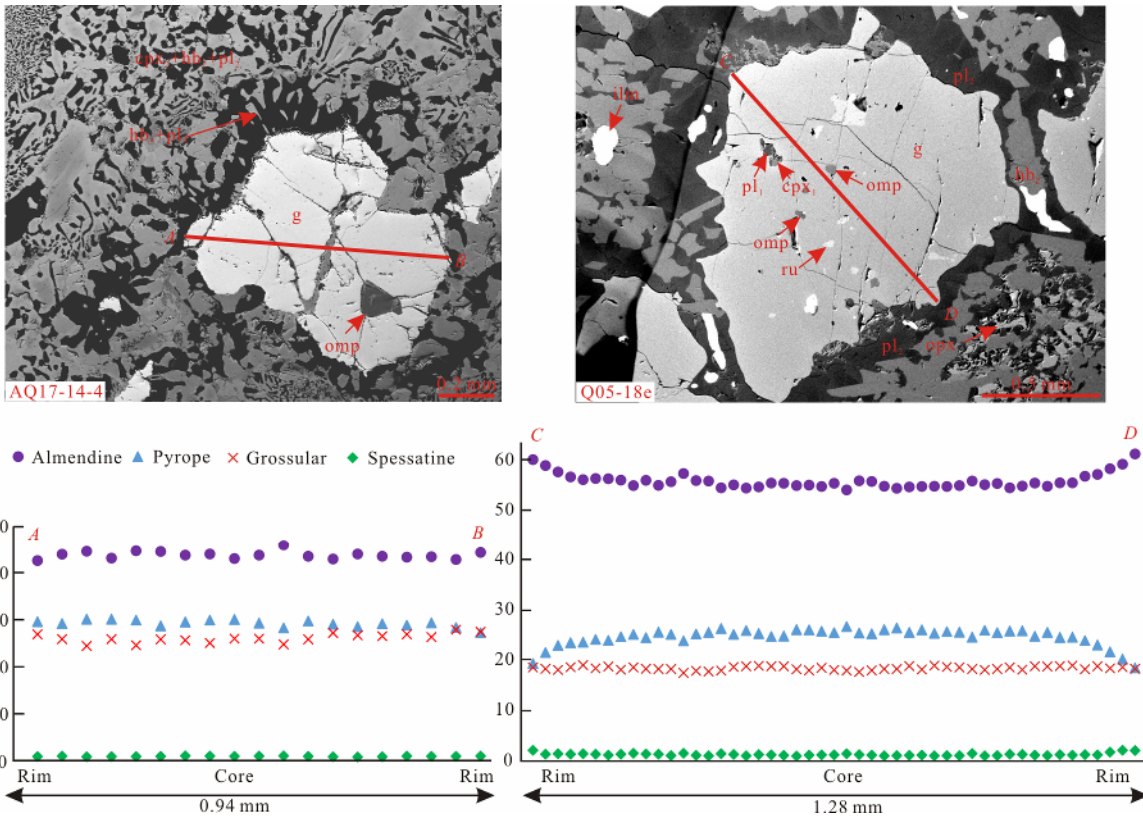


Figure 5. BSE maps and rim to rim zoning profiles of major elements of two garnet grains in samples AQ17-14-4 and Q05-18e.

2.3 Medium Pressure Granulite Facies Stage (M_3)

The MP granulite metamorphic microstructure can be divided into two types: (1) $\text{opx}+\text{pl}_2$ corona between garnet and quartz: Plagioclase forms an inner corona directly adjacent to garnet grains while orthopyroxene forms an outer corona around quartz grains (Figs. 3e, 3f, 4h). The possible metamorphic reaction is $\text{g}+\text{q}\rightarrow\text{opx}+\text{pl}$; (2) $\text{opx}+\text{pl}_2+\text{cpx}_2+\text{hb}_2$ symplectite microstructure: The texturally equilibrated matrix is composed of clinopyroxene, orthopyroxene, plagioclase and amphibole (Figs. 4f, 4g). The possible metamorphic reaction is: $\text{g}+\text{cpx}+\text{q}+\text{hb}\rightarrow\text{opx}+\text{pl}+\text{liq}$. Therefore, the resulting assemblage ($\text{g}+\text{opx}+\text{cpx}_2+\text{hb}_2+\text{q}+\text{pl}_2+\text{ilm}$) is the representative of medium pressure granulite facies assemblage.

2.4 Amphibolite Facies Stage (M_4)

The retrogressive amphibolite facies stage is characterized by hb_3+pl_3 kelyphitic rims around garnet (Figs. 3d, 3e, 4e, 4f). The intergrowths of plagioclase and hornblende on the previous minerals and the small wormlike shape indicate the cooling stage is in the mode without enough liquid. The possible metamorphic reaction is: $\text{g}+\text{cpx}+\text{q}+\text{H}_2\text{O}\rightarrow\text{pl}+\text{hb}$.

3 MINERAL CHEMISTRY

Major mineral compositions and X-ray compositional maps of garnet were obtained with a JEOL JXA 8900 electron microprobe (EMP) with a 15 kV accelerating voltage, 5 nA beam current, 5 μm probe diameter (1–2 μm for some little mineral inclusions), and count time of 10 s for peak and background, at the Laboratory of the Continental Dynamics, Institute of Geology, Chinese Academy of Geological Sciences,

Beijing. Natural or synthetic standards were used, and counts were converted to concentration using ZAF corrections. Representative mineral compositions of three granulitized eclogite samples are listed in Tables 1 and 2.

3.1 Garnet

Garnet commonly occurs as anhedral 0.5–2 mm porphyroblast with a small amount of mineral inclusions. Systematic investigation by back-scatter electron (BSE) imaging and EPMA analyses indicates garnets are almandine-rich ($\text{Alm}_{42-46}\text{Prp}_{27-30}\text{Gro}_{24-28}\text{Sps}_{0.9-2}$ in sample AQ17-14-4 and $\text{Alm}_{54-61}\text{Prp}_{20-27}\text{Gro}_{19-24}\text{Sps}_{1-2}$ in sample Q05-18e) and most garnets have homogeneous garnet cores surrounded by rims with increasing $\text{Fe}/(\text{Fe}+\text{Mg})$ (Fig. 5). These are interpreted to reflect homogenization under high temperature condition, followed by retrograde Fe/Mg re-equilibration related to volume diffusion between garnet and adjacent minerals (O'Brien, 1999).

3.2 Clinopyroxene

Clinopyroxene occurs as three textural types: anhedral inclusions within garnet porphyroblast, symplectitic clinopyroxene intergrowth with plagioclase after omphacite, and large crystals in the matrix. The single clinopyroxene inclusions in garnet are omphacite with the maximum jadeite content (33 mol%–34 mol%) which represent the M_1 stage. Some clinopyroxene inclusions intergrown with plagioclase and amphibole in garnets from three samples are omphacite with high jadeite content (21 mol%–33 mol%), whereas most clinopyroxene inclusions (cpx_1) are diopsidic clinopyroxene with low jadeite content (8 mol%–15 mol%) (Fig. 6a). Some cores of clinopyroxenes in the matrix

Table 1 Representative mineral compositions (wt.%) of samples Q07-14-4 and Q05-18e

Sample		Q07-14-4										
Mineral	g-c	g-r	cpx-in	cpx-sy	cpx-sy	opx	pl-in	pl-sy	pl-ke	amp-in	amp-sy	amp-ke
SiO ₂	40.28	39.51	54.14	51.09	51.85	54.68	57.93	57.86	59.85	42.87	45.22	44.05
TiO ₂	0.07	0.03	0.31	0.20	0.23	0.03	0.04	0.02	0.02	0.95	1.73	0.87
Al ₂ O ₃	22.4	22.08	7.20	6.34	3.40	0.99	26.32	26.61	25.28	17.66	11.55	14.20
Cr ₂ O ₃	0.03	0.05	0.06	0.03	0.05	0.04	0.00	0.04	0.02	0.03	0.18	0.07
Fe ₂ O ₃	1.25	2.43	0.65	1.01	1.79	0.30	0.18	0.41	0.19	2.51	0.61	2.27
FeO	16.22	17.48	3.93	6.31	3.74	15.86	0.00	0.00	0.00	3.52	6.92	6.25
MnO	0.40	0.57	0.07	0.07	0.13	0.28	0.04	0.01	0.00	0.08	0.09	0.13
MgO	15.33	13.62	11.87	16.90	14.17	27.33	0.02	0.03	0.03	15.53	15.48	14.75
CaO	3.34	3.74	18.84	16.73	23.52	0.40	8.33	8.89	7.28	11.89	12.06	11.52
Na ₂ O	0.00	0.02	3.39	0.70	0.63	0.01	6.74	6.13	6.95	2.50	2.21	2.50
K ₂ O	0.00	0.02	0.00	0.03	0.01	0.00	0.01	0.02	0.03	0.10	0.09	0.08
Total	99.33	99.54	100.47	99.41	99.52	99.92	99.61	100.02	99.65	97.64	96.14	96.70
Oxygen	12	12	6	6	6	6	8	8	8	23	23	23
Si	2.98	2.96	1.95	1.87	1.92	1.97	2.60	2.59	2.67	6.06	6.57	6.36
Ti	0.00	0.00	0.01	0.01	0.01	0.00	0.00	0.00	0.00	0.10	0.19	0.09
Al	1.96	1.95	0.31	0.27	0.15	0.04	1.39	1.40	1.33	2.94	1.98	2.42
Cr	0.00	0.00	0.00	0.00	0.00	0.00	0.00	0.00	0.00	0.00	0.02	0.01
Fe ³⁺	0.07	0.14	0.02	0.03	0.05	0.01	0.01	0.01	0.01	0.27	0.07	0.25
Fe ²⁺	1.01	1.09	0.12	0.19	0.12	0.48	0.00	0.00	0.00	0.42	0.84	0.76
Mn	0.03	0.04	0.00	0.00	0.00	0.01	0.00	0.00	0.00	0.01	0.01	0.02
Mg	1.69	1.52	0.64	0.92	0.78	1.47	0.00	0.00	0.00	3.27	3.35	3.17
Ca	0.27	0.30	0.73	0.66	0.93	0.02	0.40	0.43	0.35	1.80	1.88	1.78
Na	0.00	0.00	0.24	0.05	0.05	0.00	0.59	0.53	0.60	0.69	0.62	0.70
K	0.00	0.00	0.00	0.00	0.00	0.00	0.00	0.00	0.00	0.02	0.02	0.02
Sum	8.00	8.00	4.00	4.00	4.00	4.00	4.99	4.97	4.96	15.58	15.53	15.57
Sample		Q05-18e										
Mineral	g-c	g-m	g-r	cpx-in	cpx-m	opx	pl-in	pl-sy	pl-co	amp	amp	
SiO ₂	38.94	38.70	38.84	53.60	52.93	51.45	62.55	58.70	48.52	47.35	48.67	
TiO ₂	0.09	0.06	0.01	0.34	0.09	0.04	0.03	0.00	0.00	1.55	0.84	
Al ₂ O ₃	21.98	21.88	21.56	9.87	0.69	0.57	22.80	25.68	32.92	8.83	7.68	
Cr ₂ O ₃	0.00	0.00	0.02	0.01	0.01	0.00	0.00	0.00	0.00	0.05	0.07	
Fe ₂ O ₃	0.35	0.31	0.00	0.15	0.32	0.00	0.39	0.27	0.20	2.41	3.18	
FeO	24.38	24.53	26.92	5.68	10.13	29.08	0.00	0.00	0.28	12.31	11.95	
MnO	0.51	0.43	0.91	0.06	0.23	0.42	0.00	0.00	0.05	0.17	0.16	
MgO	7.02	6.77	5.17	9.49	12.81	17.24	0.02	0.01	0.02	12.34	12.88	
CaO	7.14	7.22	6.84	16.10	22.94	0.46	4.64	7.52	15.63	11.01	11.31	
Na ₂ O	0.02	0.01	0.00	4.54	0.17	0.01	8.98	7.28	2.46	1.40	0.91	
K ₂ O	0.00	0.00	0.00	0.02	0.00	0.00	0.10	0.11	0.02	0.33	0.09	
Total	100.40	99.91	100.28	99.87	100.32	99.27	99.51	99.57	100.10	97.75	97.74	
Oxygen	12	12	12	6	6	6	8	8	8	23	23	
Si	2.990	2.990	3.020	1.940	1.980	1.990	2.785	2.634	2.220	6.909	7.074	
Ti	0.010	0.000	0.000	0.010	0.000	0.000	0.001	0.000	0.000	0.170	0.092	
Al	1.990	1.990	1.980	0.420	0.030	0.030	1.197	1.358	1.780	1.519	1.316	
Cr	0.000	0.000	0.000	0.000	0.000	0.000	0.000	0.000	0.000	0.006	0.008	
Fe ³⁺	0.020	0.020	0.000	0.000	0.010	0.000	0.013	0.009	0.010	0.265	0.348	
Fe ²⁺	1.570	1.590	1.750	0.170	0.320	0.940	0.000	0.000	0.010	1.502	1.452	
Mn	0.030	0.030	0.060	0.000	0.010	0.010	0.000	0.000	0.000	0.021	0.020	
Mg	0.800	0.780	0.600	0.510	0.720	1.000	0.001	0.001	0.000	2.684	2.790	
Ca	0.590	0.600	0.570	0.620	0.920	0.020	0.221	0.362	0.770	1.721	1.761	
Na	0.000	0.000	0.000	0.320	0.010	0.000	0.775	0.633	0.220	0.396	0.256	
K	0.000	0.000	0.000	0.000	0.000	0.000	0.006	0.006	0.000	0.061	0.017	
Sum	8.000	8.000	7.990	4.000	4.000	3.990	5.000	5.000	5.000	15.254	15.134	

g-c. Garnet core; g-m. garnet mantle; g-r. garnet rim; cpx-in. clinopyroxene inclusion; cpx-sy. clinopyroxene symplectite; pl-in. plagioclase inclusion; pl-sy. plagioclase symplectite; pl-ke. plagioclase kelyphitic rim; pl-co. pl-corona; amp-in. amphibole inclusion; amp-ke. amphibole kelyphitic rim; amp-ke. The mineral data of sample Q05-18e are from Zhang et al. (2007).

Table 2 Representative mineral compositions (wt.%) of sample AQ17-14-4

Mineral	g-c	g-m	g-m	g-r	g-r	cpx-in	cpx-m	cpx-m	cpx	amp-sy	amp-co	amp-co	pl-sy	pl-co	pl-co
SiO ₂	38.92	39.30	38.57	38.60	37.58	52.8	54.06	53.50	52.78	43.18	42.30	42.35	60.30	59.84	57.01
TiO ₂	0.08	0.09	0.03	0.05	0.06	0.18	0.19	0.18	0.04	0.14	1.68	0.46	2.29	0.00	0.03
Al ₂ O ₃	20.93	20.74	21.26	21.21	21.46	7.75	7.49	7.20	2.94	2.11	12.80	15.13	14.38	24.59	24.60
Cr ₂ O ₃	0.00	0.03	0.06	0.06	0.03	0.02	0.05	0.00	0.05	0.03	0.15	0.07	0.05	0.00	0.00
Fe ₂ O ₃	2.49	1.53	2.64	2.23	4.00	4.12	0.00	0.00	0.00	0.47	2.29	3.63	2.28	0.23	0.27
FeO	18.98	19.20	18.37	18.44	17.65	1.33	5.91	7.50	8.75	8.25	13.18	9.93	11.34	0.00	0.00
MnO	0.48	0.45	0.45	0.47	0.49	0.06	0.07	0.06	0.15	0.11	0.12	0.10	0.00	0.03	0.00
MgO	7.43	7.40	7.58	7.13	6.93	10.79	10.34	10.47	13.07	13.28	10.60	11.81	11.34	0.00	0.02
CaO	10.74	10.96	10.78	11.34	11.13	17.94	17.50	18.26	21.49	22.24	11.30	10.96	11.44	6.45	7.26
Na ₂ O	0.03	0.04	0.00	0.01	0.05	4.24	3.55	2.62	0.60	0.45	2.06	2.60	2.11	7.62	7.24
K ₂ O	0.00	0.00	0.00	0.00	0.00	0.01	0.00	0.00	0.00	0.01	0.06	0.08	0.09	0.05	0.01
Total	100.08	99.74	99.74	99.54	99.38	99.24	99.16	99.79	99.87	99.32	97.19	96.71	97.54	99.24	99.51
Oxygen	12	12	12	12	12	6	6	6	6	6	23	23	23	8	8
Si	2.981	3.015	2.959	2.970	2.905	1.922	1.974	1.957	1.962	1.959	6.393	6.215	6.203	2.700	2.683
Ti	0.005	0.005	0.002	0.003	0.003	0.005	0.005	0.005	0.001	0.004	0.187	0.051	0.252	0.000	0.001
Al	1.890	1.876	1.923	1.924	1.956	0.333	0.322	0.310	0.129	0.093	2.234	2.621	2.483	1.298	1.300
Cr	0.000	0.002	0.004	0.004	0.002	0.001	0.001	0.000	0.001	0.001	0.018	0.008	0.006	0.000	0.000
Fe ³⁺	0.143	0.088	0.153	0.129	0.233	0.113	0.000	0.000	0.013	0.255	0.401	0.251	0.008	0.009	0.007
Fe ²⁺	1.216	1.232	1.179	1.187	1.141	0.041	0.180	0.229	0.272	0.259	1.632	1.221	1.389	0.000	0.000
Mn	0.031	0.029	0.031	0.032	0.002	0.002	0.005	0.003	0.015	0.015	0.012	0.012	0.000	0.001	0.000
Mg	0.848	0.846	0.867	0.817	0.798	0.585	0.563	0.571	0.724	0.742	2.339	2.586	2.475	0.000	0.001
Ca	0.881	0.901	0.886	0.935	0.922	0.700	0.685	0.716	0.856	0.893	1.793	1.725	1.795	0.309	0.349
Na	0.004	0.006	0.000	0.001	0.007	0.299	0.251	0.186	0.043	0.033	0.591	0.741	0.599	0.662	0.629
K	0.000	0.000	0.000	0.000	0.000	0.000	0.000	0.000	0.011	0.015	0.017	0.003	0.001	0.001	0.001
Sum	8.000	8.000	8.000	8.000	8.000	4.000	3.985	3.976	3.993	4.000	15.554	15.734	15.568	4.979	4.971

g-c: garnet core; g-m: garnet mantle; g-r: garnet rim; cpx-in: clinopyroxene inclusion; cpx-m: clinopyroxene symplectite; pl-in: plagioclase symplectite; pl-co: plagioclase kelyphitic rim; pl-co: pl-corona; amp-in: amphibole inclusion; amp-co: amphibole kelyphitic rim;

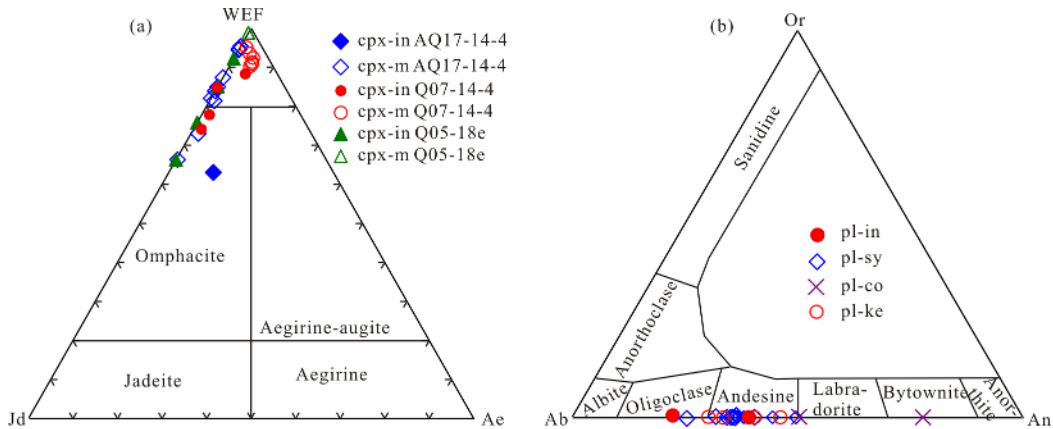


Figure 6. (a) Mineral chemistry diagrams showing the compositional variations of clinopyroxene (after Morimoto, 1988); (b) the Or-An-Ab diagram of plagioclase.

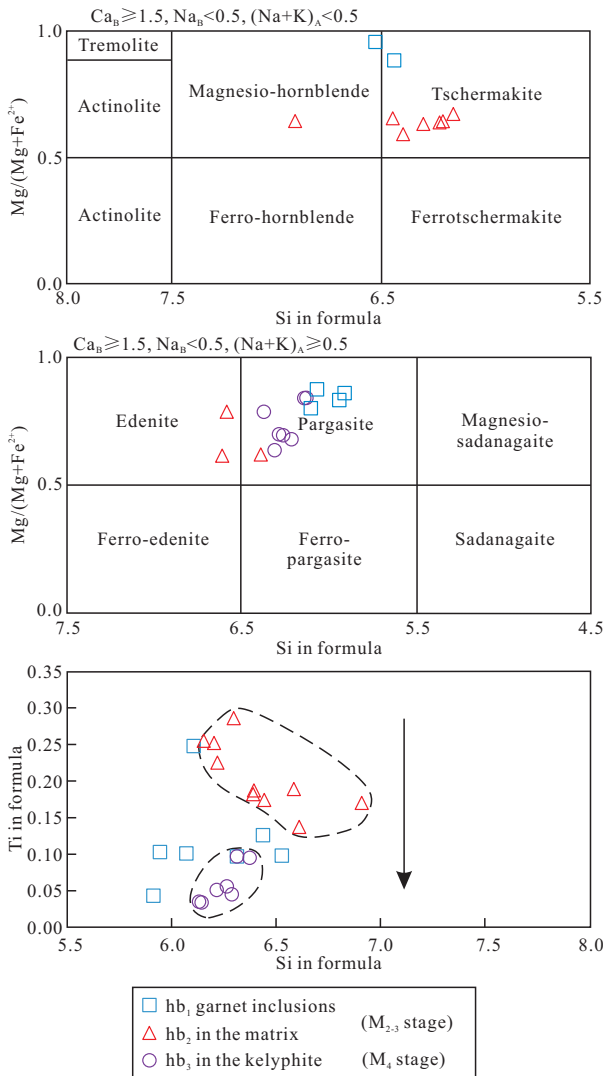


Figure 7. Mineral chemistry diagrams showing the compositional variations of amphibole (after Leake et al., 1997).

from sample AQ17-14-4 are omphacite component with 25 mol%–33 mol% of jadeite. Most clinopyroxene grains (cpx₂) in the symplectite and in the matrix are diopside with lower jadeite contents (5.5 mol%–18 mol%). The clinopyroxene intergrown with orthopyroxene in the matrix has the minimum jadeite (1.2

mol%–5.3 mol%) which represent the M₃ stage.

3.3 Orthopyroxene

Orthopyroxene occurs in the symplectites and in the matrix, and also as inclusions within garnet porphyroblast. All microstructural types of opx are enstatite-ferrosililite with Ca=0.01–0.02 p.f.u. and Fe³⁺=0.01–0.015 p.f.u. There are small compositional differences among different types of opx but obvious differences in different samples. Orthopyroxene in sample Q07-14-4 ($Mg^{\#}=0.73\text{--}0.79$) ($Mg^{\#}=Mg^{2+}/(Mg^{2+}+Fe^{2+})$) is richer in Mg than in sample Q05-18e ($Mg^{\#}=0.46\text{--}0.52$).

3.4 Plagioclase

Plagioclase as inclusion (pl₁) in garnet and symplectitic plagioclase (pl₂) associated with diopsidic clinopyroxene have compositions varying from oligoclase to andesine with a high albite content (An₂₄–₄₉) (Fig. 6b). Coronitic plagioclase (pl₂) associated with orthopyroxene is rich in anorthite with a composition ranging from labradorite to bytownite (An₅₀–₇₇). Kelyphytic plagioclase (pl₃) is andesine in composition (An₃₁–₄₆). This indicates that the anorthite content in plagioclase increases from HP granulite facies to MP granulite facies and then decreases during the cooling stage.

3.5 Amphibole

All amphibole textural varieties observed in the retrograde eclogites are calcic according to Leake et al. (1997) (Fig. 7). Most of amphibole inclusions (hb₁) within garnet porphyroblasts are pargasite and minor inclusions are tschermakite with low Si (5.9–6.5 p.f.u.). Amphiboles in the matrix (hb₂) are tschermakite and minor edenite, pargasite, magnesio-hornblende with Si=6.2–6.9 p.f.u. Kelyphytic amphiboles (hb₃) are pargasite with Si=6.1–6.4 p.f.u. and Ti=0.03–0.1 p.f.u., representing low temperature amphiboles during the cooling stage.

4 PHASE EQUILIBRIUM MODELING

Phase equilibrium diagrams were constructed using THERMOCCLC 3.45 (Powell et al., 1998; updated 2016) and the internally consistent thermodynamic dataset ds62 of Holland and Powell (2011). The a-x relations for the main phases are: metabasite melt, clinopyroxene and amphibole (Green et al., 2016); garnet, orthopyroxene, muscovite (White et al., 2014); feldspars

(Holland and Powell, 2003); ilmenite (White et al., 2000). Pure phases include quartz, rutile, aqueous fluid (H_2O). For modeling the mineral assemblages and compositions of the granulitized eclogite, the model system NCKFMASHTO ($Na_2O-CaO-K_2O-FeO-MgO-Al_2O_3-SiO_2-H_2O-TiO_2-O$, where O is a proxy for Fe_2O_3) was chosen to calculate pseudosections.

Whole-rock compositions were analyzed at the National Geological Analysis Center of China, Beijing. Oxides of major elements including loss on ignition (LOI), were determined by X-ray fluorescence (XRF) (Rigaku-3080) with an analytical uncertainty of <0.5%. Fe_2O_3 content was analyzed by XRF as TFe_2O_3 while FeO content was analyzed by potassium bichromate titrimetric method as supplement by difference. In order to obtain representative chemical compositions of the whole rock studied, more than 2 kg of each sample material was powdered.

The $P-T$ estimate of the granulite facies condition especially the temperature estimate suggests a wide gap by conventional thermobarometry. To simulate the $P-T$ condition of MP granulite facies, we chose sample Q05-18e which preserved obvious metamorphic reaction structures associated with orthopyroxene to make pseudosection. Bulk rock composition for the granulitized eclogite determined by XRF with the form of weight percentage for each oxide is presented in Table 3, the bulk rock compositions for constructing pseudosection are normalized by molar proportion. All P_2O_5 was removed, and the total CaO was proportionally adjusted to account for the chemical contribution of apatite. Mn content is neglected because the Mn content of the bulk rock composition is very low (0.26 wt.%) and Mn is mainly in spessartine. Abundant symplectites and coronas in the granulitized eclogites indicate a fluid-absent feature especially in retrograde stage. H_2O content of 2.8 mol% was constrained to be in accordance with the component feature of M_3 stage mineral assemblage and ensure that they were stable just above the solidus in the late cooling stage (e.g., Korhonen et al., 2012, 2011) (Fig. 8).

The $P-T$ pseudosection calculated for sample Q05-18e in the system NCKFMASHTO(+q) is presented in Fig. 9 and it is constructed over a range of 5–25 kbar and 650–950 °C. Garnet is stable at pressure >5.2 kbar, orthopyroxene is stable at pressure <10.2 kbar and plagioclase is stable at pressure <18.3 kbar. Hornblende is stable at temperature <940 °C. With the initial 2.8 mol% H_2O content, the pseudosection gives a fluid-absent solidus which is constrained by the appearance of liquid (melt). The temperature of the fluid-absent solidus at 5 kbar is 830 °C which is in accordance with the fluid-absent solidus of amphibolite from experimental petrology (Zhang et al., 2013; Rapp et al., 2003; Sen and Dunn, 1994; Rushmer, 1993, 1991; Beard and

Lofgren, 1991). The slope of fluid-absent solidus is plus before the orthopyroxene is out and then turns minus at high pressure without orthopyroxene. High pressure granulite transfers to eclogite after plagioclase is out when pressure rises and transfers to granulite after garnet is out when pressure declines (Green and Ringwood, 1967). The field of pseudosection can be divided into eclogite facies, high pressure granulite facies and medium-low pressure granulite facies (Fig. 10). According to the types and presence or absence of hydroites, those metamorphic facies are divided into more subfacies (Wei et al., 2017): epidote eclogite subfacies (ep-EC), amphibole eclogite subfacies (hb-EC), dry eclogite subfacies (d-EC), amphibole high pressure granulite subfacies (hb-HGN), dry high pressure granulite facies (d-HGN), amphibole medium pressure granulite subfacies (hb-MGN), dry medium pressure granulite facies (d-MGN), amphibole granulite subfacies (hb-GN), dry granulite facies (d-GN).

The pseudosection is contoured with isopleths of X_{py} of garnet, jd (cpx) and Mg (cpx) in clinopyroxene and Ca (pl) in plagioclase in Fig. 11. The X_{py} contents increase with pressure rising from g-cpx-ru-pl-q stability field to g-cpx-ru-q field and are more than 0.27 which the garnet recorded in the studied granulitized eclogite, and the minimal jd (cpx) is more than 0.35 while the biggest jd (cpx) recorded in the granulitized eclogite is 0.33. The eclogite-facies assemblage (M_1) can only constrain a relatively large $P-T$ interval at >18.5 kbar and >830 °C. The g-cpx-pl-ru-q stability field and the minimum Ca (pl) recorded in pl inclusions within garnet give a $P-T$ condition of 17.5 kbar/852–858 °C, which represents the early stage of HP granulite facies (M_{2-1}). In g-cpx-hb-pl-ru-q field, the intersections of measured jd (cpx) and Mg (cpx) isopleths in $pl_1+cpx_1+hb_1$ inclusions in garnet and $pl_2+cpx_2+hb_2$ symplectites constrains the $P-T$ conditions of 14.7 to 11.3 kbar at 858 °C for the late stage of HP granulite facies (M_{2-2}). In the g-cpx-opx-hb-pl-ilm-liq-q field, the preserved maximum X_{py} contents of inner garnet rim (0.24) associated with the maximum Ca (pl) contents (0.77–0.78) in plagioclase coronas constrain MP granulite facies condition (M_3) at 7.6–7.7 kbar/878–883 °C. The decrease of X_{py} contents in garnet rim from 0.26 to 0.19 associated with the g-opx-cpx-hb-pl-ilm stability field gives a nearly isobaric cooling route. The $P-T$ condition of amphibolite facies (M_4) is roughly estimated at $P<5$ kbar and $T<650$ °C.

5 DISCUSSION

5.1 $P-T$ Evolution of the Luliangshan Granulitized Eclogite

Although omphacite inclusions in garnet and omphacite grains in the matrix were both recognized in the Luliangshan granulitized eclogites, phase equilibrium modeling indicates that the jadeite contents of omphacite are still too low to constrain the

Table 3 Bulk compositions used for mineral equilibria modeling of sample Q05-18e

SiO_2	Al_2O_3	CaO	MgO	FeO	K_2O	Na_2O	TiO_2	Fe_2O_3	MnO	CO_2	P_2O_5	LOI	Total
wt.% (from XRF whole rock analyses)													
47.49	15.19	9.13	6.60	13.09	0.18	1.37	2.73	2.11	0.26	0.41	0.27	0.19	99.02
Normalized molar proportion (%)													
SiO_2	Al_2O_3	CaO	MgO	FeO	K_2O	Na_2O	TiO_2	O	H_2O	Total	Forms		
52.02	9.80	10.71	10.78	11.99	0.13	1.45	2.25	0.87	0.00	100.00	$M_{H_2O}(0)$		
46.82	8.82	9.64	9.70	10.79	0.11	1.31	2.02	0.78	10.00	100.00	$M_{H_2O}(1)$		
50.56	9.53	10.41	10.48	11.65	0.12	1.41	2.19	0.85	2.80	100.00	$P-T$ pseudosection		

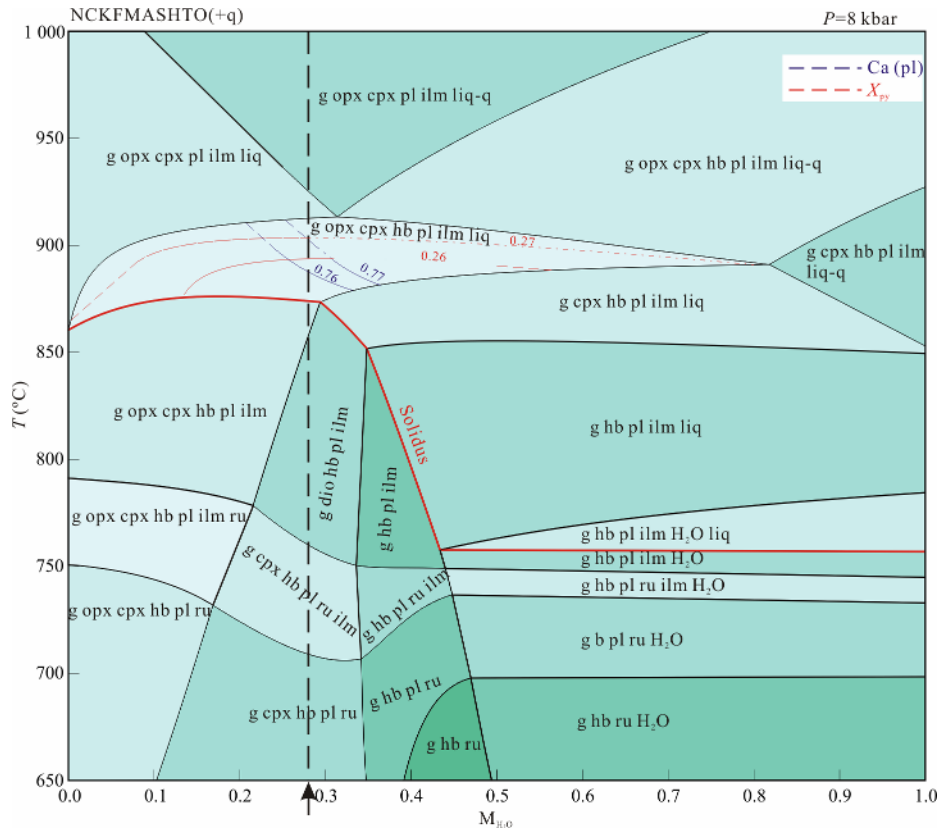


Figure 8. T - $\text{M}_{\text{H}_2\text{O}}$ diagram to constrain the H_2O contents for modeled sample Q05-18e.

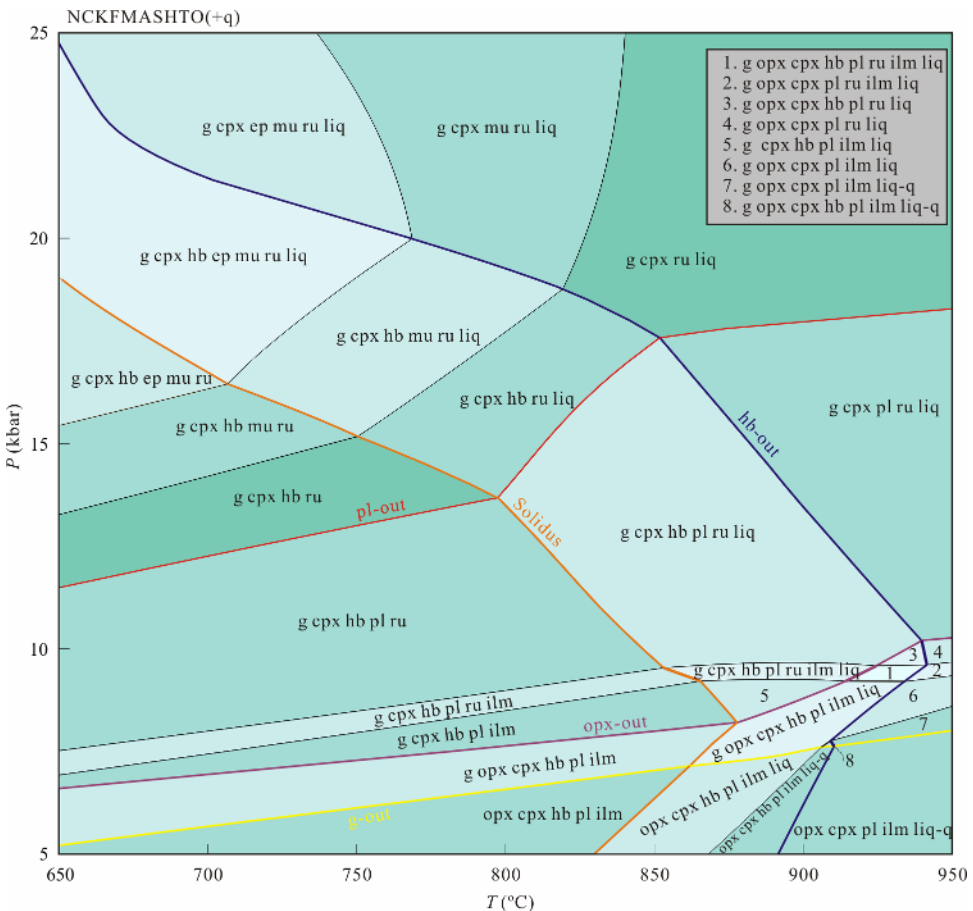


Figure 9. P - T pseudosection in the system NCKFMASHTO(+q) with XRF-based bulk-rock composition of sample Q05-18e.

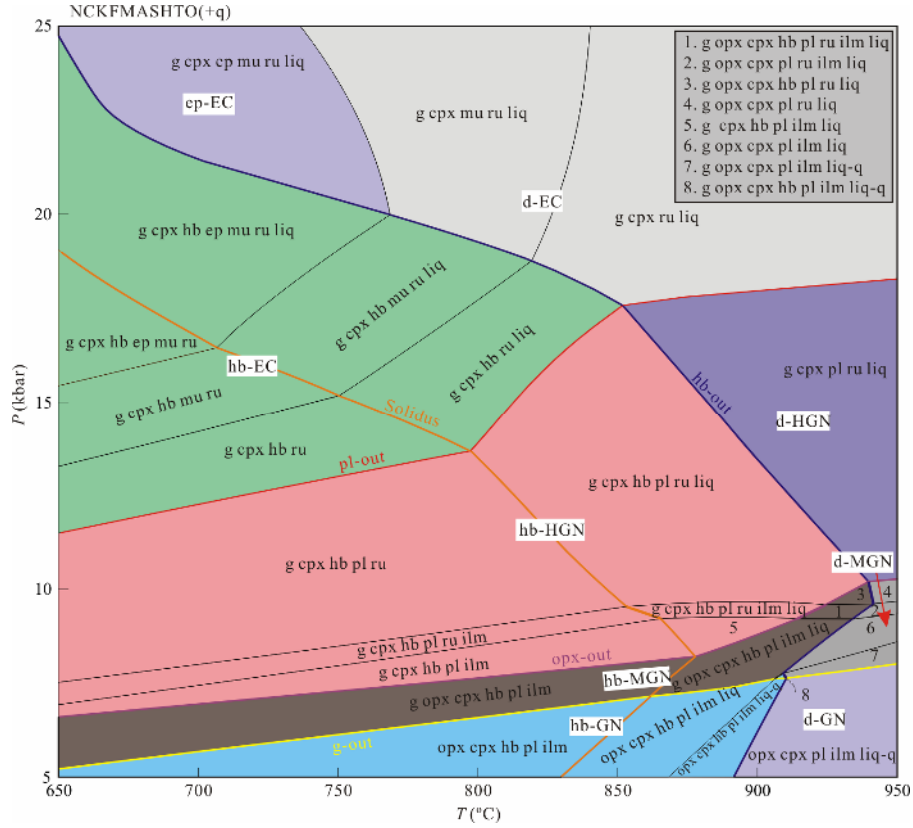


Figure 10. P - T pseudosection showing the distribution of different metamorphic subfacies. Metamorphic subfacies abbreviations: ep-EC. epidote-eclogite; hb-EC. hornblende-eclogite; d-EC. dry-eclogite; hb-HGR. hornblende-high pressure granulite; d-HGR. dry-high pressure granulite; hb-MGR. hornblende-medium pressure granulite; d-MGR. dry-medium pressure granulite; hb-GR. hornblende-granulite; d-GR. dry-pressure granulite.

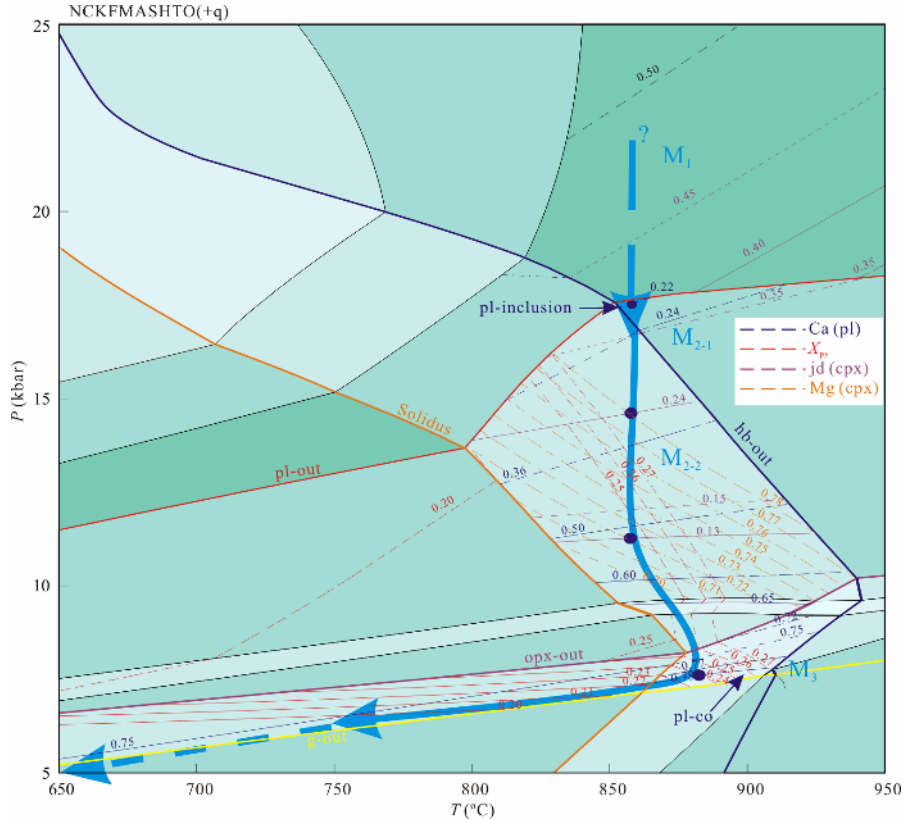


Figure 11. P - T pseudosection with the isopleths of different minerals. The isopleth notation used is: $X_{\text{py}} = \text{Mg}/(\text{Ca} + \text{Fe}^{2+} + \text{Mn} + \text{Mg})$, Ca (pl) = $\text{Ca}/(\text{Na} + \text{Ca} + \text{K})$, Mg (cpx) = $\text{Mg}/(\text{Fe}^{2+} + \text{Mg})$.

peak eclogite facies P - T condition. Those omphacites recognized in granulitized eclogite were possibly alternated and re-equilibrated in decompression stage, especially during HT granulite facies overprint. The cpx+pl symplectites are generally considered as products of omphacite breakdown during early decompression process from eclogite facies to HP granulite facies by the reaction $\text{omp}+\text{q}\rightarrow\text{cpx}+\text{pl}$ (Zhang et al., 2018; Cruciani et al., 2012; Groppe et al., 2007; Zhao et al., 2001). The eclogite facies P - T conditions were constrained at $P>18.5$ kbar and $T>830$ °C, indicating that the Luliangshan granulitized eclogites formed under a high temperature eclogite facies condition prior to granulite facies overprint. Subsequently, the g-cpx-pl-ru-q-liq stability field and the minimum Ca (pl) of plagioclase inclusions in garnet yields a P - T condition of 17.5 kbar/852–858 °C for the early HP granulite facies stage. The measured garnet component cannot be used to constrain the P - T condition of the HP granulite facies stage because of the effect of the overprint of the followed MP/HT granulite facies which leads to the homogenization of garnet. In addition, the $\text{pl}_1+\text{cpx}_1+\text{hb}_1$ inclusions in garnet which have fractures linked to the matrix and $\text{pl}_2+\text{cpx}_2+\text{hb}_2$ symplectites in the matrix both represent the HP granulite facies stage. The intersections of measured jd (cpx) and Mg (cpx) isopleths yield an ITD process from 14.7 to 11.3 kbar at 858 °C. In the late HP granulite facies stage, hornblende began to appear and the mode proportion (mol%) increases from zero to more than 30% (Fig. 12). The liquid (melt) mode proportion decreases from 8% to 3%. The P - T condition of the MP granulite facies stage (7.6–7.7 kbar,

902–907 °C) represents a process of pressure decrease and temperature increase. The microtextural observations can be explained by two metamorphic reactions: $\text{g}+\text{cpx}\rightarrow\text{opx}+\text{pl}$ and $\text{g}+\text{q}\rightarrow\text{opx}+\text{pl}$. In fact, there is a hidden reaction: $\text{hb}+\text{pl}+\text{q}\rightarrow\text{g}+\text{cpx}+\text{liq}$, which provides liquid in granulite facies condition (Wei et al., 2017). This can be recognized by the mode proportion of hornblende decreased to 30% and the mode proportion of liquid increased to 5% in the MP granulite stage (Fig. 12). The cooling stage after MP granulite facies stage is defined by the suprasolidus back-reaction $\text{g}+\text{cpx}+\text{liq}\rightarrow\text{hb}+\text{pl}+\text{q}$. The decrease of X_{py} contents in garnet rim constrained an IBC route to amphibolite facies (<5 kbar and <650 °C), which is characterized by the pl_3+hb_3 kelyphites around the garnet.

5.2 Melt Loss or not?

As a result of the retrograde metamorphic evolution involving the suprasolidus back-reactions between retention melt and residue, most granulites can only preserve their assemblages at the fluid-absent solidus and record much lower cooling temperatures (Wei et al., 2017). Granulite facies mineral assemblages are preserved due to substantial melt loss (White and Powell, 2002; Hensen and Green, 1971). The mode proportion of hornblende increased to more than 40% when temperature decreased under the solidus. The volume of hornblende is in accordance with that we observed in the samples. This indicates that the limited amount of melt almost did not lose and was transferred to hornblende by suprasolidus back-reactions. This is also in accordance with the fact that the obvious melt loss phenomenon

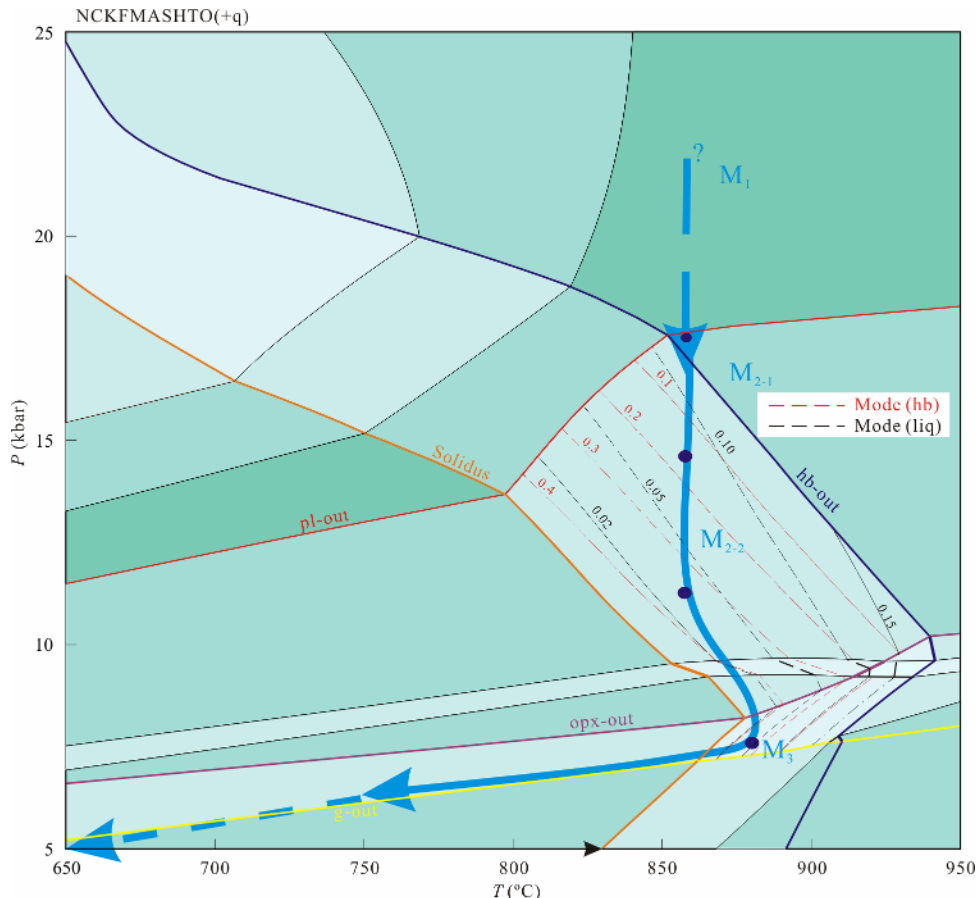


Figure 12. P - T pseudosection with the mode proportions of the melt and amphibole.

has not been observed in field outcrop scale. The Luliangshan granulitized eclogites represent a special occasion that most of melt produced in the MP granulite facies stage did not lose in cooling stage. This phenomenon can be explained by two reasons: (1) the MP granulite facies assemblage was transferred from eclogite facies and HP granulite facies assemblages; (2) the fluid-absent condition. The $\text{opx}+\text{pl}_2$ were mainly produced by reaction $\text{g}+\text{cpx}_2+\text{q}\rightarrow\text{opx}+\text{pl}_2$, which represents the decompression reaction under fluid-absent condition (Wei et al., 2017). The limited amount of melt (~5%) was far smaller than the amount of pelite granulite (>30%) (e.g., Cai et al., 2014) and the suprasolidus back-reaction $\text{g}+\text{cpx}+\text{liq}\rightarrow\text{hb}+\text{pl}+\text{q}$ could not consume all clinopyroxene. Therefore, the Luliangshan granulitized eclogites preserved the MP granulite facies assemblage $\text{g}+\text{opx}+\text{cpx}_2+\text{pl}_2+\text{ilm}+\text{q}$ although the limited melt did not loss during the cooling stage.

5.3 H_2O Content and Effective Bulk Composition for Granulitized Eclogites

Although a clockwise P - T path and a typical IBC cooling process were constrained by the initial bulk rock composition and limited H_2O content, there are still several issues need to explain for the H_2O content and bulk rock composition for different stages. As mentioned above, the Luliangshan granulitized eclogites recorded eclogite facies stage, HP granulite stage, MP granulite stage and amphibolite stage. Most mineral assemblages are only domainal equilibrium assemblages. The garnet and clinopyroxene formed in eclogite facies stage were modified in retrograde stage. The initial bulk rock composition may be not very critical to simulate the MP granulite stage by phase diagram modeling. On the other hand, the H_2O content of the bulk rock composition was constrained by T - H_2O diagram which mainly simulate the cooling process but cannot represent H_2O condition of the HP granulite stage. Although petrographic feature also indicates a fluid-absent condition for the HP granulite stage, it may be the result of the melt loss in peak eclogite facies stage considering the eclogite facies temperature is very high (>850 °C). Therefore, more precise P - T estimations of different stages for the Luliangshan granulitized eclogites should be based on the effective bulk composition from domainal equilibrium zone and also consider the possible melt loss in eclogite facies stage.

5.4 P - T - t Path

Combining petrological data with zircon U-Pb datings of the granulitized gneisses and associated mafic granulite (granulitized eclogites) in the Luliangshan terrane, three metamorphic stages, including eclogite facies (>450 Ma), HP granulite facies (ca. 450 Ma) and MP granulite facies (ca. 425 Ma) were suggested (Zhang et al., 2008, 2007). U-Pb datings of zircons with plagioclase, clinopyroxene, rutile and garnet inclusions in zircons constrain the HP granulite facies stage at ca. 450 Ma, and zircons with plagioclase, orthopyroxene and garnet inclusions constrain the MP granulite facies stage at ca. 425 Ma (Zhang et al., 2008). The timing of amphibolite facies stage was also obtained as 415–382 Ma in the Luliangshan terrane (Chen et al., 2018) from the same outcrop as sample AQ17-14-4. Combining the previous chronological data with our P - T estimates, a new P - T - t path was refined for the Luli-

angshan granulitized eclogites (Fig. 13). The results based on the P - T pseudosections and the isopleths modeling are consistent with the modes and compositions of the observed mineral assemblages, and give a clockwise P - T - t path which is defined by an ITD process from the eclogite facies to HP granulite facies, and then a slight temperature rising to MP granulite facies stage followed by a nearly IBC process. Our estimates of the MP granulite temperatures (878–883 °C) are slightly higher than those estimates by conventional thermobarometry (Chen et al., 2018; Cao et al., 2017; Zhang et al., 2008, 2007). Because of the fast cation diffusion under high-temperature conditions and the absence of the role that partial melting commonly plays, the application of mineral compositions to thermobarometry may underestimate the peak temperature of granulites (Powell and Holland, 2008; Frost and Chacko, 1989; Harley, 1989). In contrast, pseudosection thermobarometry usually yields higher peak temperature estimates based on the stability field of the peak assemblage with relevant isopleths of mineral compositions and modal proportions because it uses the assemblage as the basis for estimating P - T conditions which is less prone to post-peak modification than mineral compositions (e.g., Li and Wei, 2016; Morrissey et al., 2014; Yin et al., 2014; Korhonen et al., 2013; Shimizu et al., 2013; White and Powell, 2002). Therefore, the P - T path constrained by pseudosection analysis with the latest melt modal for mafic rocks should be more reliable than those by conventional thermobarometry (Green et al., 2016).

5.5 Tectonic Implications

The present and previous data show the Luliangshan terrane is a “hot” HP-UHP terrane, in contrast to the adjacent Yuka-Luofengpo terrane which is characterized by low-medium temperature-ultrahigh pressure peak metamorphic condition (566–680 °C and 2.35–3.4 GPa) and the following low-medium temperature retrograde conditions mainly in amphibolite field (10–16 kbar and 580–630 °C) (Ren et al., 2018, 2017; Zhang G B et al., 2009; Chen et al., 2005; Zhang J X et al., 2005, 2004) (Fig. 13). This suggests that the Luliangshan terrane and adjacent Yuka-Luofengpo terrane do not maintain structural coherence and represent different metamorphic slices. The Luliangshan terrane has a prolonged exhumation history and slow exhumation rates and underwent a widespread anatexis, which may partially and completely obliterate the direct evidence of eclogite facies metamorphism. In addition, the Luliangshan granulitized eclogites recorded higher eclogite facies temperature than that from the Yuka-Luofengpo eclogites. This possibly implies that the Luliangshan eclogites may be closer to the mantle wedge than the adjacent Yuka-Luofengpo terrane and therefore formed under higher geothermal gradient condition during continental subduction. The record of HP granulite facies (~450 Ma) and MP granulite facies (~425 Ma) of the Luliangshan granulitized eclogites and associated granulitized gneiss indicates that the Luliangshan slice was relaminated to the root part of the thickened lower crust related to the Early Paleozoic continental collision between the Qilian (or Oulongbuluke micro-continent block) and Qaidam blocks and was overprinted by the HP granulite facies metamorphism. The following exhumation of the Luliangshan terrane to relatively shallow crustal levels was accompanied by re-equilibration under MP granulite facies conditions during

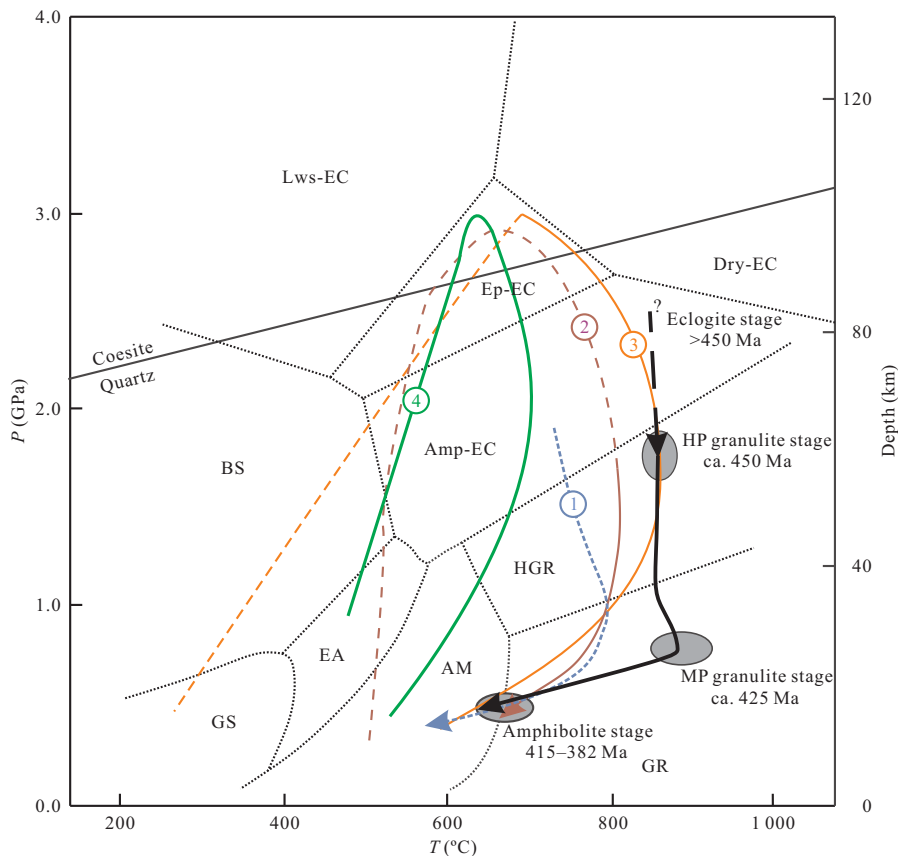


Figure 13. P - T - t path of the granulitized eclogites and associated rocks from the Luliangshan terrane. P - T path 1 from Zhang et al. (2008) for the metamorphic evolution of the Luliangshan granulitized gneiss and associated mafic granulite. P - T path 2 after Cao et al. (2017) for a granulitized eclogite. P - T path 3 after Chen et al. (2018) for the Luliangshan granulitized eclogite. P - T path 4 after Zhang et al. (2009) for the Yuka eclogite.

a period of protracted continental collision. The scenario is analogous to the UHP/HP rocks recorded medium pressure Barrovian metamorphic event overprint in typical collisional orogens such as the west Western Gneiss Region (Walsh and Hacker, 2004), the Devonian–Carboniferous European Variscides (O’Brien, 1997) and southern Sulu (Nakamura and Hirajima, 2000). The regional Barrovian metamorphic overprint event may be related to the thermal relaxation during the late collisional orogenic stage. The regional Barrovian metamorphism can be also connected to the contemporary magmatism. The adjacent granite intrusion to the west of the Luliangshan terrane also records a similar emplacement age (~428 Ma) to that of the medium pressure Barrovian metamorphic event. It was interpreted as the product of partial melting of sedimentary rocks from the subduction continental crust during exhumation stage (Zhang et al., 2017; Meng and Zhang, 2008).

6 CONCLUSIONS

(1) Petrologic data and phase equilibrium modeling suggest a multi-stage metamorphic history of the granulitized eclogites in the Luliangshan terrane: (1) an eclogite facies metamorphism ($P>18.5$ kbar, $T>830$ °C) characterized by relic omphacite in the matrix and within garnet; (2) a protracted high pressure granulite facies stage (11.3–17.5 kbar and 852–858 °C); (3) the later medium pressure granulite facies stage (7.6–7.7 kbar and 878–883 °C); and (4) a retrogressive amphibolite facies stage ($P<5$ kbar and $T<650$ °C)

(2) The present data show that the Luliangshan terrane is a “hot” HP-UHP terrane. The direct evidence of eclogite facies metamorphism has been partially and completely obliterated during a period of protracted continental collision.

ACKNOWLEDGMENTS

We are most grateful to two reviewers for critical and constructive reviews for the manuscript. This work was financially supported by the National Natural Science Foundation of China (Nos. 41630207, 41572180) and the China Geological Survey (No. DD20160022). The final publication is available at Springer via <https://doi.org/10.1007/s12583-019-0897-6>.

REFERENCES CITED

- Beard, J. S., Lofgren, G. E., 1991. Dehydration Melting and Water-Saturated Melting of Basaltic and Andesitic Greenstones and Amphibolites at 1, 3, and 6.9 kb. *Journal of Petrology*, 32(2): 365–401. <https://doi.org/10.1093/petrology/32.2.365>
- Cai, J., Liu, F. L., Liu, P. H., et al., 2014. Metamorphic P - T Path and Tectonic Implications of Pelitic Granulites from the Daqingshan Complex of the Khondalite Belt, North China Craton. *Precambrian Research*, 241: 161–184. <https://doi.org/10.1016/j.precamres.2013.11.012>
- Cao, Y. T., Liu, L., Chen, D. L., et al., 2017. Partial Melting during Exhumation of Paleozoic Retrograde Eclogite in North Qaidam, Western China. *Journal of Asian Earth Sciences*, 148: 223–240. <https://doi.org/10.1016/j.jseas.2017.09.009>
- Chen, D. L., Sun, Y., Liu, L., et al., 2005. Metamorphic Evolution of the

- Yuka Eclogite in the North Qaidam, NW China: Evidences from the Compositional Zonation of Garnet and Reaction Texture in the Rock. *Acta Petrologica Sinica*, 21(4): 1039–1048 (In Chinese with English Abstract)
- Chen, X., Xu, R. K., Zheng, Y. Y., et al., 2018. Petrology and Geochemistry of High Niobium Eclogite in the North Qaidam Orogen, Western China: Implications for an Eclogite Facies Metamorphosed Island Arc Slice. *Journal of Asian Earth Sciences*, 164: 380–397. <https://doi.org/10.1016/j.jseas.2018.07.003>
- Cruciani, G., Franceschelli, M., Groppo, C., et al., 2012. Metamorphic Evolution of Non-Equilibrated Granulitized Eclogite from Punta de Li Tulchi (Variscan Sardinia) Determined through Texturally Controlled Thermodynamic Modelling. *Journal of Metamorphic Geology*, 30(7): 667–685. <https://doi.org/10.1111/j.1525-1314.2012.00993.x>
- Frost, B. R., Chacko, T., 1989. The Granulite Uncertainty Principle: Limitations on Thermobarometry in Granulites. *Journal of Geology*, 97(4): 435–450. <https://doi.org/10.1086/629321>
- Green, D. H., Ringwood, A. E., 1967. An Experimental Investigation of the Gabbro to Eclogite Transformation and Its Petrological Applications. *Geochimica et Cosmochimica Acta*, 31(5): 767–833. [https://doi.org/10.1016/s0016-7037\(67\)80031-0](https://doi.org/10.1016/s0016-7037(67)80031-0)
- Green, E. C. R., White, R. W., Diener, J. F. A., et al., 2016. Activity-Composition Relations for the Calculation of Partial Melting Equilibria in Metabasic Rocks. *Journal of Metamorphic Geology*, 34(9): 845–869. <https://doi.org/10.1111/jmg.12211>
- Groppi, C., Lombardo, B., Rolfo, F., et al., 2007. Clockwise Exhumation Path of Granulitized Eclogites from the Ama Drime Range (Eastern Himalayas). *Journal of Metamorphic Geology*, 25(1): 51–75. <https://doi.org/10.1111/j.1525-1314.2006.00678.x>
- Groppi, C., Rolfo, F., Liu, Y. C., et al., 2015. P-T Evolution of Elusive UHP Eclogites from the Luotian Dome (North Dabie Zone, China): How far can the Thermodynamic Modeling Lead Us?. *Lithos*, 226: 183–200. <https://doi.org/10.1016/j.lithos.2014.11.013>
- Harley, S. L., 1989. The Origins of Granulites: A Metamorphic Perspective. *Geological Magazine*, 126(3): 215–247. <https://doi.org/10.1017/s0016756800022330>
- Hensen, B. J., Green, D. H., 1971. Experimental Study of the Stability of Cordierite and Garnet in Pelitic Compositions at High Pressures and Temperatures. *Contributions to Mineralogy and Petrology*, 33(4): 309–330. <https://doi.org/10.1007/bf00382571>
- Holland, T. J. B., Powell, R., 1998. An Internally Consistent Thermodynamic Data Set for Phases of Petrological Interest. *Journal of Metamorphic Geology*, 16(3): 309–343. <https://doi.org/10.1111/j.1525-1314.1998.00140.x>
- Holland, T. J. B., Powell, R., 2011. An Improved and Extended Internally Consistent Thermodynamic Dataset for Phases of Petrological Interest, Involving a New Equation of State for Solids. *Journal of Metamorphic Geology*, 29(3): 333–383. <https://doi.org/10.1111/j.1525-1314.2010.00923.x>
- Holland, T. J. B., Powell, R., 2003. Activity-Composition Relations for Phases in Petrological Calculations: An Asymmetric Multicomponent Formulation. *Contributions to Mineralogy and Petrology*, 145(4): 492–501. <https://doi.org/10.1007/s00410-003-0464-z>
- Korhonen, F. J., Brown, M., Clark, C., et al., 2013. Osumilite-Melt Interactions in Ultrahigh Temperature Granulites: Phase Equilibria Modelling and Implications for the P-T-t Evolution of the Eastern Ghats Province, India. *Journal of Metamorphic Geology*, 31(8): 881–907. <https://doi.org/10.1111/jmg.12049>
- Korhonen, F. J., Powell, R., Stout, J. H., 2012. Stability of Sapphirine+Quartz in the Oxidized Rocks of the Wilson Lake Terrane, Labrador: Calculated Equilibria in NCKFMASHTO. *Journal of Metamorphic Geology*, 30(1): 21–36. <https://doi.org/10.1111/j.1525-1314.2011.00954.x>
- Korhonen, F. J., Saw, A. K., Clark, C., et al., 2011. New Constraints on UHT Metamorphism in the Eastern Ghats Province through the Application of Phase Equilibria Modelling and *in situ* Geochronology. *Gondwana Research*, 20(4): 764–781. <https://doi.org/10.1016/j.gr.2011.05.006>
- Leake, B. E., Woolley, A. R., Arps, C. E. S., et al., 1997. Nomenclature of Amphiboles; Report of the Subcommittee on Amphiboles of the International Mineralogical Association Commission on New Minerals and Mineral Names. *Mineralogical Magazine*, 61(405): 295–310. <https://doi.org/10.1180/minmag.1997.061.405.13>
- Li, X. W., Wei, C. J., 2016. Phase Equilibria Modelling and Zircon Age Dating of Pelitic Granulites in Zhaojiayao, from the Jining Group of the Khondalite Belt, North China Craton. *Journal of Metamorphic Geology*, 34(6): 595–615. <https://doi.org/10.1111/jmg.12195>
- Li, Y. S., Zhang, J. X., Mostofa, K. M. G., et al., 2018. Petrogenesis of Carbonatites in the Luliangshan Region, North Qaidam, Northern Tibet, China: Evidence for Recycling of Sedimentary Carbonate and Mantle Metasomatism within a Subduction Zone. *Lithos*, 322: 148–165. <https://doi.org/10.1016/j.lithos.2018.10.010>
- Liao, X. Y., Liu, L., Wang, Y. W., et al., 2016. Multi-Stage Metamorphic Evolution of Retrograde Eclogite with a Granulite-Facies Overprint in the Zhaigen Area of the North Qinling Belt, China. *Gondwana Research*, 30: 79–96. <https://doi.org/10.1016/j.gr.2015.09.012>
- Meng, F. C., Zhang, J. X., 2008. Contemporaneous of Early Palaeozoic Granite and High Temperature Metamorphism, North Qaidam Mountains, Western China. *Acta Petrologica Sinica*, 24(7): 1585–1594 (in Chinese with English Abstract)
- Morimoto, N., 1988. Nomenclature of Pyroxenes. *Mineralogy and Petrology*, 39(1): 55–76. <https://doi.org/10.1007/bf01226262>
- Morrissey, L. J., Hand, M., Raimondo, T., et al., 2014. Long-Lived High-T, Low-P Granulite Facies Metamorphism in the Arunta Region, Central Australia. *Journal of Metamorphic Geology*, 32(1): 25–47. <https://doi.org/10.1111/jmg.12056>
- Nakamura, D., Hirajima, T., 2000. Granulite-Facies Overprinting of Ultrahigh-Pressure Metamorphic Rocks, Northeastern Su-Lu Region, Eastern China. *Journal of Petrology*, 41(4): 563–582. <https://doi.org/10.1093/petrology/41.4.563>
- O'Brien, P. J., 1999. Asymmetric Zoning Profiles in Garnet from HP-HT Granulite and Implications for Volume and Grain-Boundary Diffusion. *Mineralogical Magazine*, 63(2): 227–238. <https://doi.org/10.1180/002646199548457>
- O'Brien, P. J., 1997. Garnet Zoning and Reaction Textures in Overprinted Eclogites, Bohemian Massif, European Variscides: A Record of Their Thermal History during Exhumation. *Lithos*, 41(1/2/3): 119–133. [https://doi.org/10.1016/s0024-4937\(97\)82008-7](https://doi.org/10.1016/s0024-4937(97)82008-7)
- Powell, R., Holland, T. J. B., 2008. On Thermobarometry. *Journal of Metamorphic Geology*, 26(2): 155–179. <https://doi.org/10.1111/j.1525-1314.2007.00756.x>
- Powell, R., Holland, T. J. B., Worley, B., 1998. Calculating Phase Diagrams Involving Solid Solutions via Non-Linear Equations, with Examples Using THERMOCALC. *Journal of Metamorphic Geology*, 16(4): 577–588. <https://doi.org/10.1111/j.1525-1314.1998.00157.x>
- Rapp, R. P., Shimizu, N., Norman, M. D., 2003. Growth of Early Continental Crust by Partial Melting of Eclogite. *Nature*, 425(6958): 605–609. <https://doi.org/10.1038/nature02031>
- Ren, Y. F., Chen, D. L., Kelsey, D. E., et al., 2018. Metamorphic Evolution of a Newly Identified Mesoproterozoic Oceanic Slice in the Yuka Terrane and Its Implications for a Multi-Cyclic Orogenic History of the

- North Qaidam UHPM Belt. *Journal of Metamorphic Geology*, 36(4): 463–488. <https://doi.org/10.1111/jmg.12300>
- Ren, Y. F., Chen, D. L., Kelsey, D. E., et al., 2017. Petrology and Geochemistry of the Lawsonite (Pseudomorph)-Bearing Eclogite in Yuka Terrane, North Qaidam UHPM Belt: An Eclogite Facies Metamorphosed Oceanic Slice. *Gondwana Research*, 42: 220–242. <https://doi.org/10.1016/j.gr.2016.10.011>
- Rushmer, T., 1991. Partial Melting of Two Amphibolites: Contrasting Experimental Results under Fluid-Absent Conditions. *Contributions to Mineralogy and Petrology*, 107(1): 41–59. <https://doi.org/10.1007/bf00311184>
- Rushmer, T., 1993. Experimental High-Pressure Granulites: Some Applications to Natural Mafic Xenolith Suites and Archean Granulite Terranes. *Geology*, 21(5): 411–414. [https://doi.org/10.1130/0091-7613\(1993\)021<411:ehpgsa>2.3.co;2](https://doi.org/10.1130/0091-7613(1993)021<411:ehpgsa>2.3.co;2)
- Sen, C., Dunn, T., 1994. Dehydration Melting of a Basaltic Composition Amphibolite at 1.5 and 2.0 GPa: Implications for the Origin of Adakites. *Contributions to Mineralogy and Petrology*, 117(4): 394–409. <https://doi.org/10.1007/bf00307273>
- Shimizu, H., Tsunogae, T., Santosh, M., et al., 2013. Phase Equilibrium Modelling of Palaeoproterozoic Ultrahigh-Temperature Sapphirine Granulite from the Inner Mongolia Suture Zone, North China Craton: Implications for Counterclockwise P-T Path. *Geological Journal*, 48(5): 456–466. <https://doi.org/10.1002/gj.2504>
- Song, S. G., Yang, J. S., Xu, Z. Q., et al., 2003. Metamorphic Evolution of the Coesite-Bearing Ultrahigh-Pressure Terrane in the North Qaidam, Northern Tibet, NW China. *Journal of Metamorphic Geology*, 21(6): 631–644. <https://doi.org/10.1046/j.1525-1314.2003.00469.x>
- Song, S. G., Zhang, L. F., Niu, Y. L., et al., 2006. Evolution from Oceanic Subduction to Continental Collision: A Case Study from the Northern Tibetan Plateau Based on Geochemical and Geochronological Data. *Journal of Petrology*, 47(3): 435–455. <https://doi.org/10.1093/petrology/egi080>
- Song, S. G., Niu, Y. L., Su, L., et al., 2014. Continental Orogenesis from Ocean Subduction, Continent Collision/Subduction, to Orogen Collapse, and Orogen Recycling: The Example of the North Qaidam UHPM Belt, NW China. *Earth-Science Reviews*, 129: 59–84. <https://doi.org/10.1016/j.earscirev.2013.11.010>
- Song, S. G., Su, L., Li, X. H., et al., 2012. Grenville-Age Orogenesis in the Qaidam-Qilian Block: The Link between South China and Tarim. *Precambrian Research*, 220/221: 9–22. <https://doi.org/10.1016/j.precamres.2012.07.007>
- Song, S. G., Su, L., Li, X. H., et al., 2010. Tracing the 850-Ma Continental Flood Basalts from a Piece of Subducted Continental Crust in the North Qaidam UHPM Belt, NW China. *Precambrian Research*, 183(4): 805–816. <https://doi.org/10.1016/j.precamres.2010.09.008>
- Song, S. G., Zhang, L. F., Niu, Y. L., 2004. Ultra-Deep Origin of Garnet Peridotite from the North Qaidam Ultrahigh-Pressure Belt, Northern Tibetan Plateau, NW China. *American Mineralogist*, 89(8/9): 1330–1336. <https://doi.org/10.2138/am-2004-8-922>
- Song, S. G., Zhang, L. F., Niu, Y. L., et al., 2005. Geochronology of Diamond-Bearing Zircons from Garnet Peridotite in the North Qaidam UHPM Belt, Northern Tibetan Plateau: A Record of Complex Histories from Oceanic Lithosphere Subduction to Continental Collision. *Earth and Planetary Science Letters*, 234(1/2): 99–118. <https://doi.org/10.1016/j.epsl.2005.02.036>
- Walsh, E. O., Hacker, B. R., 2004. The Fate of Subducted Continental Margins: Two-Stage Exhumation of the High-Pressure to Ultrahigh-Pressure Western Gneiss Region, Norway. *Journal of Metamorphic Geology*, 22(7): 671–687. <https://doi.org/10.1111/j.1525-1314.2004.00541.x>
- Wei, C. J., Guan, X., Dong, J., 2017. HT-UHT Metamorphism of Metabasites and the Petrogenesis of TTGs. *Acta Petrologica Sinica*, 33(5): 1381–1404 (in Chinese with English Abstract)
- White, R. W., Powell, R., 2002. Melt Loss and the Preservation of Granulite Facies Mineral Assemblages. *Journal of Metamorphic Geology*, 20(7): 621–632. https://doi.org/10.1046/j.1525-1314.2002.00206_20_7.x
- White, R. W., Powell, R., Holland, T. J. B., et al., 2014. New Mineral Activity-Composition Relations for Thermodynamic Calculations in Metapelite Systems. *Journal of Metamorphic Geology*, 32(3): 261–286. <https://doi.org/10.1111/jmg.12071>
- White, R. W., Powell, R., Holland, T. J. B., et al., 2000. The Effect of TiO₂ and Fe₂O₃ on Metapelite Assemblages at Greenschist and Amphibolite Facies Conditions: Mineral Equilibria Calculations in the System K₂O-FeO-MgO-Al₂O₃-SiO₂-H₂O-TiO₂-Fe₂O₃. *Journal of Metamorphic Geology*, 18(5): 497–511. <https://doi.org/10.1046/j.1525-1314.2000.00269.x>
- Yang, J. J., Zhu, H., Deng, J. F., et al., 1994. The Discovery of Garnet Peridotite in Northern Chaidam Mountains and Its Significance. *Acta Petrologica et Mineralogica*, 13(2): 97–105 (in Chinese with English Abstract)
- Yang, J. S., Xu, Z. Q., Zhang, J. X., et al., 2002. Early Palaeozoic North Qaidam UHP Metamorphic Belt on the North-Eastern Tibetan Plateau and a Paired Subduction Model. *Terra Nova*, 14(5): 397–404. <https://doi.org/10.1046/j.1365-3121.2002.00438.x>
- Yang, J. S., Xu, Z. Q., Li, H. B., et al., 1998. The Eclogites have been Found in the Northern Qaidam Basin, Western China. *Chinese Science Bulletin*, 43(14): 1544–1549 (in Chinese)
- Yang, J. S., Xu, Z. Q., Song, S. G., et al., 2001. Discovery of Coesite in the North Qaidam Early Palaeozoic Ultrahigh Pressure (UHP) Metamorphic Belt, NW China. *Acta Geologica Sinica*, 75(2): 175–179 (in Chinese with English Abstract)
- Yang, J. Z., Liu, X. C., Wu, Y. B., et al., 2015. Zircon Record of Ocean-Continent Subduction Transition Process of Dulan UHPM Belt, North Qaidam. *Journal of Earth Science*, 26(5): 617–625. <https://doi.org/10.1007/s12583-015-0585-0>
- Yin, C. Q., Zhao, G. C., Wei, C. J., et al., 2014. Metamorphism and Partial Melting of High-Pressure Pelitic Granulites from the Qianlidian Complex: Constraints on the Tectonic Evolution of the Khondalite Belt in the North China Craton. *Precambrian Research*, 242: 172–186. <https://doi.org/10.1016/j.precamres.2013.12.025>
- Yu, S. Y., Zhang, J. X., Li, H. K., et al., 2013. Geochemistry, Zircon U-Pb Geochronology and Lu-Hf Isotopic Composition of Eclogites and Their Host Gneisses in the Dulan Area, North Qaidam UHP Terrane: New Evidence for Deep Continental Subduction. *Gondwana Research*, 23(3): 901–919. <https://doi.org/10.1016/j.gr.2012.07.018>
- Zhang, C., Holtz, F., Koepke, J., et al., 2013. Constraints from Experimental Melting of Amphibolite on the Depth of Formation of Garnet-Rich Restites, and Implications for Models of Early Archean Crustal Growth. *Precambrian Research*, 231: 206–217. <https://doi.org/10.1016/j.precamres.2013.03.004>
- Zhang, C., van Roermund, H., Zhang, L. F., et al., 2012. A Polyphase Metamorphic Evolution for the Xitieshan Paragneiss of the North Qaidam UHP Metamorphic Belt, Western China: *In-situ* EMP Monazite- and U-Pb Zircon SHRIMP Dating. *Lithos*, 136–139: 27–45. <https://doi.org/10.1016/j.lithos.2011.07.024>
- Zhang, G. B., Ellis, D. J., Christy, A. G., et al., 2009. UHP Metamorphic Evolution of Coesite-Bearing Eclogite from the Yuka Terrane, North Qaidam UHPM Belt, NW China. *European Journal of Mineralogy*, 21(6): 1287–1300. <https://doi.org/10.1127/0935-1221/2009/0021-1989>
- Zhang, J. X., Meng, F. C., Yang, J. S., 2004. Eclogitic Metapelites in the Western Segment of the North Qaidam Mountains: Evidence on “in

- situ*" Relationship between Eclogite and Its Country Rock. *Science in China Series D: Earth Sciences*, 47(12): 1102–1112. <https://doi.org/10.1360/02yd0311>
- Zhang, J. X., Yang, J. S., Mattinson, C. G., et al., 2005. Two Contrasting Eclogite Cooling Histories, North Qaidam HP/UHP Terrane, Western China: Petrological and Isotopic Constraints. *Lithos*, 84(1/2): 51–76. <https://doi.org/10.1016/j.lithos.2005.02.002>
- Zhang, J. X., Meng, F. C., Yu, S. Y., 2007. Metamorphic History Recorded in High Pressure Mafic Granulites in the Luliangshan Mountains to the North of Qaidam Basin, Northwest China: Evidence from Petrology and Zircon SHRIMP Geochronology. *Earth Science Frontiers*, 14(1): 85–97 (in Chinese with English Abstract)
- Zhang, J. X., Mattinson, C. G., Meng, F., et al., 2008. Polyphase Tectono-thermal History Recorded in Granulitized Gneisses from the North Qaidam HP/UHP Metamorphic Terrane, Western China: Evidence from Zircon U-Pb Geochronology. *Geological Society of America Bulletin*, 120(5/6): 732–749. <https://doi.org/10.1130/b26093.1>
- Zhang, J. X., Mattinson, C. G., Yu, S. Y., et al., 2010. U-Pb Zircon Geochronology of Coesite-Bearing Eclogites from the Southern Dulan Area of the North Qaidam UHP Terrane, Northwestern China: Spatially and Temporally Extensive UHP Metamorphism during Continental Subduction. *Journal of Metamorphic Geology*, 28(9): 955–978. <https://doi.org/10.1111/j.1525-1314.2010.00901.x>
- Zhang, J. X., Yu, S. Y., Mattinson, C. G., 2017. Early Paleozoic Polyphase Metamorphism in Northern Tibet, China. *Gondwana Research*, 41: 267–289. <https://doi.org/10.1016/j.gr.2015.11.009>
- Zhang, Y. H., Wei, C. J., Lu, M. J., et al., 2018. *P-T-t* Evolution of the High-Pressure Mafic Granulites from Northern Hengshan, North China Craton: Insights from Phase Equilibria and Geochronology. *Precambrian Research*, 312: 1–15. <https://doi.org/10.1016/j.precamres.2018.04.022>
- Zhao, G. C., Cawood, P. A., Wilde, S. A., et al., 2001. High-Pressure Granulites (Retrograded Eclogites) from the Hengshan Complex, North China Craton: Petrology and Tectonic Implications. *Journal of Petrology*, 42(6): 1141–1170. <https://doi.org/10.1093/petrology/42.6.1141>